Title: Regulatory network structure determines patterns of intermolecular epistasis

Authors:

Mato Lagator[1], Srdjan Sarikas[1], Hande Acar[1], Jonathan P. Bollback[1,2]*, Călin C. Guet[1]*

Affiliations:

[1] IST Austria, Am campus 1, 3400 Klosterneuburg, Austria

[2] Institute of Integrative Biology, University of Liverpool, Liverpool, Merseyside, UK

Corresponding author

Călin C. Guet

Telephone number: +43 2243 9000 4001

Email address: calin@ist.ac.at

*co-corresponding authors

Keywords:

Distributions of mutational effects; epistasis; gene regulation; *Escherichia coli*

Abstract

Most phenotypes are determined by molecular systems composed of specifically interacting molecules. However, unlike for individual components, little is known about the distributions of mutational effects of molecular systems as a whole. We ask how the distribution of mutational effects of a transcriptional regulatory system differs from the distributions of its components, by first independently, and then simultaneously, mutating a transcription factor and the associated promoter it represses. We find that the system distribution exhibits increased phenotypic variation compared to individual component distributions - an effect arising from intermolecular epistasis between the transcription factor and its DNA-binding site. In large part, this epistasis can be qualitatively attributed to the structure of the transcriptional regulatory system, and could therefore be a common feature in prokaryotes. Counter-intuitively, intermolecular epistasis can alleviate the constraints of individual components, thereby increasing phenotypic variation that selection could act on and facilitating adaptive evolution.

Introduction

Distributions of mutational effects (DMEs) and the nature of the interactions among mutations (epistasis) critically determine evolutionary paths and outcomes (Eyre-Walker and Keightley 2007; de Visser and Krug 2014). DMEs are central to a range of fundamental questions in evolutionary biology (Halligan and Keightley 2009), including understanding the origins of novel traits (Soskine and Tawfik 2010), evolution of sex and recombination (Otto and Lenormand 2002), and maintenance of genetic variation (Charlesworth *et al.* 1995). In contrast to selective constraints, which act on the variation already present in a population, biophysical laws and molecular mechanisms that define how a molecular system functions constrain the access to phenotypic variation through mutation (Camps *et al.* 2007; Wagner 2011), and in doing so determine the shape of the DME (Fontana and Buss 1994).

Even though most phenotypes are determined by underlying molecular systems that consist of multiple specifically interacting molecular components, direct and systematic experimental estimates of DMEs have been limited to the two extremes only: either at the level of the whole organism, obtained in mutation accumulation studies (Halligan and Keightley 2009); or at the level of individual components, such as proteins (Wang *et al.* 2002; Bershtein *et al.* 2006; Sarkisyan *et al.* 2016) and DNA-binding sites for transcription factors (Kinney *et al.* 2010; Shultzaberger *et al.* 2012; Yun *et al.* 2012; Metzger *et al.* 2015), determined through direct mutagenesis. Knowing only the effects of mutations in individual molecular components might be insufficient to understand how the whole system evolves, as recent studies focusing on the interaction of mutations in two components of a molecular system uncovered the existence of pervasive intermolecular epistasis (Anderson *et al.* 2015; Podgornaia and Laub 2015). Because of the large

mutational space of proteins, these studies focused only on mutations in specific residues that lie at the interface between the two interacting molecules. In contrast, addressing the more general question of how intermolecular epistasis shapes DMEs of molecular systems is only possible by experimentally tackling the nearly prohibitive space of possible mutational combinations, which even for single components is conceivable only in rare cases (Sarkisyan *et al.* 2016). Here, by using one of the best understood transcriptional regulation systems, we experimentally ask how the DME of a system differs from the DMEs of its constitutive components.

To address this question, we used a simple gene regulatory system based on the canonical Lambda bacteriophage switch (Ptashne 2011), consisting of three components – the σ^{70} RNA polymerase complex (together, we refer to them as RNAP), transcription factor CI (*trans*-element), and the P_R *cis*-element that contains the overlapping DNA-binding sites of the two proteins (Fig.1). These three molecular components interact to produce a quantitative phenotype: gene expression. Specifically, we used a genetic system in which a strong promoter P_R controls the expression of a yellow fluorescence protein (*yfp*), and is repressed by the CI repressor, which we placed under the inducible promoter P_{TET} (Fig.1B,C). This system exhibits high *yfp* expression in the absence of CI, where the level of expression is determined solely by RNAP binding. However, in the presence of CI, achieved by the induction of the P_{TET} promoter, the system is strongly repressed (Fig.2A). We find that, even in such a simple transcriptional regulatory system, the DME of the system differs unexpectedly from the individual component DMEs, and that most of this difference can be directly attributed to the genetic regulatory structure of the system.

Results

To determine the DMEs of individual components in our system, we performed direct mutagenesis on the *cis*- and the *trans*-element independently. For each component, we created libraries with approximately 0.01, 0.04, and 0.07 mutations per nucleotide (low, intermediate, and high mutation probability libraries, respectively). Due to the different sizes of the two components (84bp for *cis* and 714bp for *trans*), mutants in *cis*-element libraries contained on average 1, 3, and 6 mutations, while mutants in *trans*-element libraries contained on average 7, 28, and 49 mutations, respectively. We did not mutate the σ^{70} – RNAP complex due to its cell-wide pleiotropic effects. For assessing the DMEs of the system, we created three additional 'system mutant libraries' by combining *cis*- and *trans*-element mutant libraries of the same mutation probability. Each library consisted of more than 30,000 uniquely transformed individuals, and we estimated the corresponding DME for each library by measuring fluorescence, i.e. gene expression, of one million randomly sampled individuals by flow cytometry. We quantified the differences in DMEs in two ways. First, by observing the frequency of mutants in three biologically meaningful categories (Fig.2A): (i) mutants that are indistinguishable from the wildtype without the CI repressor ('high expression phenotypes'); (ii) mutants indistinguishable from the wildtype with CI ('no expression phenotypes'); and, importantly for our argument, (iii) mutants with expression levels that the wildtype cannot achieve ('intermediate expression phenotypes'). Second, by calculating the Shannon entropy, which quantifies how uniformly the mutants cover the entire range of possible gene expression phenotypes.

DMEs of the *cis*- and the *trans*-element are categorically different

The difference between the effects of mutations in the *cis*- (Fig.2B,C,D) and the *trans*-element (Fig.2E,F,G) is unambiguous. Most *cis*-element mutants, in the presence of CI, have low expression (Fig.2B,C,D). Such low expression can result either from sufficient CI

126 repressor binding and/or impaired RNAP binding. The frequency of mutants with an
127 intermediate expression phenotype in the presence of CI increases with the average number
128 of mutations, a pattern that is also observed in *cis*-element libraries in the absence of CI
129 (Fig.2 - Figure Supplement 1B,C,D). In contrast, the effects of mutations in the *trans*-
130 element have a distinctive bimodal distribution (Fig.2E,F,G). The two peaks in the
131 distribution correspond to the expression levels of the wildtype population in the absence
132 and presence of CI, revealing that the majority of CI mutants are either fully or close to
133 fully functional, or completely inactive on the wildtype *cis* background. Furthermore,
134 increasing the average number of mutations in the *trans*-element decreases the frequency of
135 intermediate expression phenotypes. As the shape of the DME is determined by the
136 underlying biophysical and mechanistic constraints that limit the phenotypic variation
137 accessible through mutation, we conclude that the *cis*- and the *trans*-element have
138 categorically different constraints. This categorical difference is best observed in a direct
139 comparison between high mutation *cis* (Fig.2D) and low mutation *trans* (Fig.2E) libraries,
140 which have approximately the same average number of mutations.
141
142 In order to further demonstrate that this categorical difference is not an artifact of the
143 different number of mutations introduced into each element, we show that the same general
144 trend is evident when comparing the effects of 150 random single point mutations of
145 known identity in each, the *cis*- and the *trans*-element (Fig.2 – Figure Supplement 2A,B).
146 These measurements were done at the population level, in a plate reader. Point mutations in
147 the *cis*-element, when only their effect on RNAP binding is measured, show a high
148 frequency of intermediate expression levels. This is in agreement with other studies of
149 prokaryotic (Kinney *et al.* 2010) and eukaryotic (Shultzaberger *et al.* 2012) DNA-binding
150 sites. Similarly, we find a bimodal distribution of single mutation effects in the *trans*-

element CI, which has previously been reported for other transcription factors (Pakula *et al.* 1986; Markiewicz *et al.* 1994) and enzymes (Jacquier *et al.* 2013), and may be a common feature of proteins that are close to their optimum (Soskine and Tawfik 2010; Bataillon and Bailey 2014).

Mutating the whole system increases phenotypic variation

The DMEs for the system, in which both the *cis*- and the *trans*-element are mutated simultaneously, show a surprising pattern: a higher frequency of intermediate phenotypes compared to either of the individual component DMEs (Fig.2H,I,J). This pattern can also be observed in the library of 150 random system double mutants (Fig.2 – Figure Supplement 2), which consist of a unique combination of the previously described point mutations in *cis* and in *trans* (comparing system to *cis*: D_{KS} = 0.39, P<0.0001; system to *trans*: D_{KS} = 0.66, P<0.0001). Furthermore, the frequency of intermediate phenotypes increased with the average number of mutations (Fig.2). At intermediate and high mutation probabilities, the Shannon entropy of the system DMEs was also greater than the entropy of either of its constitutive components (Fig.2; Fig.2 – Figure Supplement 3), indicating that mutating the whole system gives rise to a more uniform range of possible phenotypes. The existence of a difference between system DMEs in the absence (Fig.2 – Figure Supplement 1H,I,J) and in the presence of repressor CI (Fig.2H,I,J) indicates that a substantial portion of mutant CIs exhibit binding to the mutated *cis*-element backgrounds, and are thus functional repressors that specifically recognize operator mutants.

We tested if the observed differences between the system and the component DMEs might arise from differences in the gene expression noise of mutants - if the system mutants have greater noise, they could also lead to an increase in the frequency of intermediate

phenotypes. However, this is unlikely as, for every mutation probability, we observed no difference in gene expression noise in our flow cytometry measurements (measured as the coefficient of variation) between 20 randomly selected system, *cis*, and *trans* mutants in the presence of CI (Fig.2 – Figure Supplement 4;5;6). Furthermore, gene expression noise was constant between all 180 random isolates (60 isolates from each of the three mutation probabilities) irrespective of their mutation probability (Fig.2 – Source Data 1).

Intermolecular epistasis drives the increase in phenotypic variation

We wanted to understand if the observed increase in the abundance of intermediate phenotypes when the whole system mutates (Fig.2) can be attributed to epistatic interactions between mutations in the *cis*- and the *trans*-element. Since we use $\log_{10}$ of expression as our phenotype of interest, we calculate epistasis between mutations in the two components of the system (what we call intermolecular epistasis) as the deviation from the additive prediction based on single component effects. The additive null prediction for interactions between mutations, when considering only three possible categories of mutational effects ('no', 'intermediate', and 'high expression'), is shown in Table 1. The standard approach of extending these predictions to whole distributions requires a convolution of individual component DMEs (Orr 2003; Lee *et al.* 2010). To obtain this 'naïve' null prediction, we convolved the observed *trans*-element DME (shown in Fig.2E,F,G) with the distribution showing how mutations in *cis* alter wildtype expression (for further details, see Materials and Methods). Note that effectively no mutations in *cis* or *trans* decrease expression relative to the wildtype, resulting in a 'naïve' system prediction exhibiting an increase in the frequency of mutants with high expression phenotypes, as seen in Fig.2H,I,J. We find that 'naïve' convolution predictions, which are carried out in the absence of any knowledge of the genetic regulatory structure of the system, are significantly different from the observed

system distributions (Fig.2H,I,J), suggesting the existence of intermolecular epistasis between the two components.

To further show that intermolecular epistasis between the *cis*- and the *trans*-element is a common feature of our system that shapes DMEs not only at elevated mutation rates but also when only a single point mutation is present in each of the components, we utilized the previously described 150 random system double mutants (Fig.2 – Figure Supplement 2), which consist of a unique combination of a single point mutation in *cis* and a single point mutation in *trans* (Fig.3 – Figure Supplement 1; Fig.3 – Source Data 1). In a plate reader, and hence at the level of a monoclonal population, we measured expression levels of all 150 system double mutants, as well as their corresponding single mutants, in the presence of CI (Fig.2 – Figure Supplement 2). From these measurements, we calculated epistasis as the deviation from the additive expectation based on wildtype-normalized single mutant effects. This definition of epistasis mirrors the convolution approach utilized for the analysis of DMEs in Fig.2.

Intermolecular epistasis was common between single point mutations in our system, as 71 of 150 double mutants significantly deviated from their additive expectations (Fig.3, Fig.3 – Figure Supplement 2). As such, intermolecular epistasis impacts expression levels in the system not only when a relatively large number of mutations accumulate, as shown in Fig.2, but also when a single point mutation is introduced in each of the components. Furthermore, 53 of these 71 mutants were in positive epistasis, meaning that the double mutant effect was higher than expected based on single mutant effects. Such positive epistasis contributes to the observed increase in the frequency of mutants with intermediate phenotypes in the system (Fig.2 – Figure Supplement 2), as seemingly neutral *trans*

mutations, which fully repress the wildtype *cis*, show elevated expression on mutated *cis* backgrounds. On the other hand, the presence of negative epistasis indicates a penetrant *trans* mutation, whose high expression on the wildtype *cis* is decreased on a mutated *cis* background. Such epistasis most frequently arises from loss of function *trans* mutations, in which the system expression level in the presence of CI is determined only by the effect of the *cis* mutation in the absence of CI. Consequently, we observed negative epistasis in eight of ten *trans* single point mutants that exhibited no measurable repression (Fig.3 – Source Data 2). We did not identify any relationship between the presence of intermolecular epistasis and the physical location of mutations in the *trans*- ($\chi^2_{(4)}$ = 2.02; P=0.73) or the *cis*-element ($\chi^2_{(5)}$ = 1.69; P=0.89)(Fig.3 – Source Data 1), indicating that even though individually mutations in some loci have a greater effect on expression level, they are not associated with any particular form of epistasis.

Intermolecular epistasis arises from the genetic regulatory structure of the system

In the system we study, the genetic regulatory structure (Fig.1) indicates that mutations in *cis* affect both the binding of RNAP and of the repressor. A comparison to the 'naïve' convolutions performed without accounting for this regulatory structure (Fig.2) demonstrates that the presence of intermolecular epistasis prevents accurate predictions of system DME from individual component DMEs. We wanted to understand if these predictions could be improved by accounting for the effects of *cis*-element mutations on RNAP binding, which are measured in the absence of CI. In other words, we wanted to connect the basic knowledge of the regulatory structure of the system to the epistasis between mutations in the two components.

To do so experimentally, we combined the high mutation probability *cis* and the low mutation probability *trans*-element libraries (Fig.4). We chose these two libraries because they have similar expected number of mutations ($n \sim 6$), therefore minimizing a potential bias in their mutational effects arising from the difference in the number of mutations in the two components. We used FACS to partition the mutant libraries into the three phenotypic bins (no expression, intermediate, and high expression, as in Fig.2). In this manner we partitioned two libraries: the high mutation *cis*-element library in the absence of CI (Fig.2 – Figure Supplement 1D) and the low mutation *trans*-element library in the presence of CI (Fig.2E). We constructed nine new mutant libraries with all possible combinations of these partitions (Fig.5A-I). From these combination DMEs, measured in the presence of CI, we calculated the expected frequencies of mutants in each of the three categories, by weighting each combination DME by the relative frequency of the original *trans*-element partition it was derived from. Then, the predicted frequency in each category of the system DME is the sum of the weighted counts in the corresponding category across all nine DMEs (see Methods). These predicted frequencies were not different from the observed ones (Table 2). As such, only by experimentally accounting for the genetic regulatory structure of the system (Fig.1) can we accurately predict mutant frequencies in three biologically meaningful categories and qualitatively explain how the *cis* background alters the phenotypic effects of *trans*-element mutations, as detailed in the legend to Fig.5.

We also produced a mathematical prediction of the system DME that incorporated the knowledge of its genetic regulatory structure. To do so, in addition to incorporating the knowledge of the effects of *cis* mutations in the absence of CI, we also assumed that all *trans*-element mutations that have high expression (same expression as the wildtype in the absence of CI) are loss-of-function mutants, which do not bind any mutated *cis*. When

convolving the two component distributions, the effects of such loss-of-function *trans* mutants are removed and replaced by the *cis*-element DME in the absence of CI. This approach, which accounts for the effects of *cis* mutations on RNAP binding, captures the frequencies of mutants in the three phenotypic categories ('no', 'intermediate', and 'high' expression) more accurately than the 'naïve' convolutions (Fig.4; Table 2; Fig.2 – Figure Supplement 7). From a theoretical evolutionary perspective, it is the deviations from a simple additive model that have well-documented consequences for organismal evolution, as they determine the ruggedness of the adaptive landscape (de Visser and Krug 2014). Here, we show how those deviations emerge from the underlying genetic regulatory structure, and hence how they might lead to better predictions of regulatory system DMEs.

Accounting for the genetic regulatory structure of the system does not explain all intermolecular epistasis

While considering the effects of *cis*-element mutations on RNAP binding explains intermolecular epistasis to an extent that allows more accurate predictions of system DMEs, it might not explain all of it. To determine the extent to which intermolecular epistasis cannot be explained by accounting for the genetic regulatory structure of the system, we constructed a second library of 150 system double mutants. This time, instead of randomly combining point mutations in *cis*- and *trans*-elements, we combined point mutations with a specific phenotype. Namely, all *cis*-element point mutants exhibited high expression in the absence of CI, meaning that the binding of RNAP was not measurably impaired (Fig.6 – Figure Supplement 1A). All point mutations in *trans* used to assemble the 150 double mutants exhibited no expression (Fig.6 – Figure Supplement 1B), meaning that these mutants had a fully functional *trans*-element on the wildtype *cis* background. The system double mutant library made in this manner corresponds to the partition combination

shown in Fig.5C. In such a library, in the presence of CI, the additive null model predicts that a double mutant would exhibit the same phenotype as its *cis* point mutant, when the corresponding *trans* mutant maintains the same binding properties as the wildtype CI. When this is true, the system double mutant would not be in significant epistasis. Conversely, the system double mutant in this library would be in significant epistasis only when the *trans* mutant binds the mutated *cis* differently than the wildtype *trans* does.

We found that 15 double mutants in this library are in significant epistasis (Fig.6). These mutants maintained a decreased yet substantial dynamical range between the two environments (absence and presence of CI), and hence were still functional regulators (Fig.6 – Source Data 1). Furthermore, all 15 were in positive epistasis, indicating that the double mutant effect is greater than the additive expectation. In such mutants, *trans* mutations are phenotypically neutral on the wildtype *cis*, but not on a mutated *cis* background, meaning that the *trans* mutant binds the mutated *cis* less strongly than the wildtype CI does. It is worth noting that the lack of mutants that are in negative epistasis in this library might be due to the strong wildtype binding of the CI repressor, so that introducing point mutations in *trans* that improve binding is highly unlikely. When mutations in *trans* induce alterations to the binding properties of the repressor (but not complete loss of function), intermolecular epistasis cannot be accounted for by the underlying structure of the genetic regulatory network. Interestingly, a disproportionate number of double mutants that were in positive epistasis carried a *trans* mutation in the linker region of the CI ($\chi^2_{(4)} = 20.66$; $P<0.0005$), which connects the N-terminal DNA binding domain with the C-terminal dimerization domain (Fig.6 – Figure Supplement 2; Fig.6 – Source Data 2). This is in contrast to the random double mutant library (Fig.3), where we found no relationships between location of mutation and epistasis.

Discussion:

In this study, we show that mutating a molecular system with the most common transcriptional regulatory structure in prokaryotes (Salgado *et al.* 2013), namely a repressible promoter, increases phenotypic variation beyond what can be achieved by mutating any of the individual components alone. We focused on the phenotypic effects, rather than the fitness effects of mutations, in order to minimize the complexity of the studied system and also to enable a more direct interpretation of the results, as fitness effects of mutations depend on a much larger, and often unknown, set of factors than simply their phenotypic effects. Doing so enables an interpretation of observed DMEs in the light of their underlying molecular mechanisms, as recently shown for a prokaryotic (Lagator *et al.* 2017) and a eukaryotic *cis*-regulatory element (White *et al.* 2016). Furthermore, while previous studies investigated the effects of specific mutations in the contact surface between two molecules (Anderson *et al.* 2015; Podgornaia and Laub 2015), their local nature, imposed by the large mutational space of proteins, prevented conclusions about DMEs of molecular systems. Precisely because our experimental approach allowed us to overcome these obstacles, we were able to show how the regulatory network structure determines intermolecular epistasis, indicating a broad range of conditions under which the additive null models of interactions between mutations might be inaccurate.

The observed increase in the frequency of intermediate phenotypes arises, in large part, from intermolecular epistasis between the two components of the system, most of which can be attributed to the structure of the gene regulatory system. The observed increase is due to both positive and negative epistasis. When intermolecular epistasis is positive, mutations in *cis* expose the genetic variation hidden in originally phenotypically neutral

trans mutations. This can be achieved in two ways: (i) through changes in the RNAP and repressor binding sites, which are accounted for by considering the genetic regulatory structure of the system (Fig.5); or (ii) when mutations in *trans* change the binding preference of the repressor, so that a mutation in *cis* decreases the binding of the mutated *trans* more than it decreases the binding of the wildtype repressor (Fig.6). Negative intermolecular epistasis, on the other hand, arises when: (i) the *trans* mutations are penetrant, so that their effects (in particular, increased expression) are buffered by mutations in *cis*. This epistasis is frequently observed when *trans* mutations lead to a complete loss of binding (high expression phenotype), so that the system phenotype becomes the same in the presence and in the absence of CI (Fig.3). In other words, the system undergoes a qualitative transition from a three-component and thus a regulated promoter, to a two-component or a constitutive promoter. Under these conditions, the system phenotype is determined only by the effect of *cis* mutations on RNAP binding, and can be thus explained by considering the genetic regulatory structure of the system (Fig.5). (ii) Negative epistasis can also arise when *trans*-element mutations alter the binding preference of the repressor, so that the mutated *trans* binds mutated *cis* more strongly than the wildtype repressor does. We found no evidence for this type of epistasis in the library of 150 random double mutants, likely due to our use of the Lambda P_R promoter, which binds the repressor very tightly.

In the studied system, we demonstrate that intermolecular epistasis is present even between single point mutations in the *cis*- and the *trans*-element (Fig.3), and not only when a larger number of mutations accumulates in each component (Fig.2). When considering interactions between point mutations (Fig.3;6), we identified that positive epistasis contributes disproportionately to the increase in the frequency of intermediate phenotypes.

The extent to which positive, as opposed to negative, epistasis drives the observed increase in the intermediate phenotypes when a greater number of mutations are present in the components (Fig.2) cannot be addressed without knowing the effects of specific molecular interactions between a prohibitively large number of mutation combinations.

Epistasis has been shown to impose constraints on evolutionary paths by increasing the ruggedness of the adaptive landscape both in theoretical and experimental studies (Whitlock *et al.* 1995; Barton and Partridge 2000; Weinreich *et al.* 2006; Poelwijk *et al.* 2011; Breen *et al.* 2012; Podgornaia and Laub 2015). Our data suggests that, for transcriptional regulatory networks, mutating the system of specifically interacting components alleviates the biophysical and mechanistic constraints acting on individual components, and in doing so increases phenotypic variation accessible through mutation. This role of intermolecular epistasis as a facilitator rather than a constraint on evolution arises, in significant part, directly from the genetic structure of a repressible transcriptional regulatory system. As such, it might be a common feature in prokaryotes, where repression through direct binding site overlap with RNAP forms the most common type of transcriptional regulatory system organization (Salgado *et al.* 2013). In these and other similar systems, potential paths for protein evolution might be more abundant when the interacting DNA-binding site is also mutating, as mutations in the partner component can expose the genetic variation hidden in originally phenotypically neutral mutations. Such intermolecular epistasis could give rise to punctuated protein evolution (Fontana and Schuster 1998) – long periods of phenotypic stasis during which a transcription factor accumulates neutral mutations, interrupted by rapid adaptive evolution facilitated by mutations in the DNA-binding site. Furthermore, a gene might be horizontally transferred with its cognate *cis*-element, but without its cognate regulator. Then, intermolecular

epistasis between the transferred *cis*-element and the orthologous transcription factor may reveal previously unavailable phenotypes that can facilitate adaptation to new niches. Therefore, accumulating mutations in the entire system, as opposed to only in a single component, appears to facilitate evolution both by extending the neutral sequence space, and hence increasing diversity through drift (Lynch and Hagner 2015), as well as by increasing the available phenotypic variability.

Materials and Methods

Gene regulation in the Lambda phage switch

The *right* regulatory region of Lambda phage (O_R) is responsible for the decision-making between lysis or lysogeny (Johnson *et al.* 1981). The regulatory region consists of two RNA polymerase (RNAP) binding sites - promoters P_R and P_{RM} (not shown), and three CI/Cro transcription factor operators (O_{R1}, O_{R2}, and O_{R3}) (Fig.1A). In the wildtype system, the strong promoter P_R leads to expression of the transcription factor Cro. The transcription factor CI represses P_R promoter by direct binding-site competition with RNAP.

Synthetic system

We used a synthetic system based on the Lambda phage switch, in which we decoupled the *cis*- and *trans*-regulatory elements (Fig.1B,C). We removed *cI* and substituted *cro* with *venus-yfp* (Nagai *et al.* 2002) under control of P_R promoter, followed by a T1 terminator sequence. The O_{R3} site was removed in order to remove the P_{RM} promoter. Separated by a terminator sequence and 500 random base pairs, we placed *cI* under the control of P_{TET}, an inducible promoter regulated by TetR (Lutz and Bujard 1997), followed by a TL17 terminator sequence. In this way, concentration of CI transcription factor in the cell was

under external control, achieved by addition of the inducer anhydrotetracycline (aTc). The entire cassette was inserted into a low-copy number plasmid backbone pZS* carrying a kanamycin resistance gene (Lutz and Bujard 1997). In this system, *cI* constitutes the *trans*-element, while the P_R promoter together with the two CI operator sites O_{R1} and O_{R2} make the *cis*-element.

Creating the mutant libraries

The library of *cis*- and *trans*-element mutants was created using the GeneMorph II™ random mutagenesis kit (Agilent Technologies, Santa Clara, US). We created three mutant libraries with different average probability of mutations (0.01, 0.04, and 0.07 mutation chance per nucleotide) for both the transcription factor (714bp) and the P_R *cis*-regulatory element (84bp). Therefore, the average number of mutations per mutant in the *trans*-element libraries was 7, 28, or 49, while in the *cis*-element it was 1, 3, or 6, respectively. We applied the same likelihood of mutation per nucleotide rather than using the same actual number of mutations between equivalent *cis*- and *trans*-element libraries in order to more accurately represent the biological process of mutagenesis.

PCR products of mutagenesis reactions were ligated into the wildtype construct, and inserted into One-Shot® Top10 cells (Life Technologies, Carlsbad, US). This step was used to maximize the library diversity due to One-Shot® Top10 cells' high competency. Following electroporation, cells were plated at low concentrations on selective kanamycin plates to allow single colony formation and minimize resource competition, and grown overnight. Using chilled LB media, colonies were washed off the plates and collected. To ensure large coverage, we cloned mutagenized PCR products until we obtained at least 30,000 individual colonies (uniquely transformed individuals). Due to the stochastic nature

of the mutagenesis protocol used (Agilent Technologies), the number of uniquely transformed individuals did not necessarily equal the number of different mutant genotypes, especially at low mutation rates. To illustrate, when the mutation rate was low so that a *cis*-element mutant would have on average only 1 mutation, some PCR mutagenesis products did not contain any mutations. When mutations were in the *trans*-element, which is ~10-fold longer, almost all PCR mutagenesis products contained several mutations. Using the information provided by the supplier (which we verified by sequencing 40 mutants from each *cis* and *trans* library, see below) on the distributions of the number of mutations (given a mutagenesis rate), we estimated that approximately 34.2%, 3.5%, and 0.2% of the low, intermediate, and high mutation number *cis*-element libraries consisted of wildtype genotypes. The comparative proportion of wildtype genotypes in the *trans*-element libraries was 0.07%, 10^{-13}%, and 10^{-22}%.

Populations containing a mixture of mutants with a given number of mutations were used to isolate plasmids, and clone them into the modified MG1655 strain expressing *tetR* gene from a constitutive PN_{25} promoter. We showed that the distributions of mutation numbers in 40 isolated individuals from each library conformed to the distributions of mutation numbers provided by the supplier. We did this by comparing the actual distribution of the number of mutations to the Poisson distribution based on the predicted mutation probability, using a Kolmogorov-Smirnov (K-S) test (Fig.2 – Source Data 2). We used a power test to determine that the sample size of 40 was sufficient to verify the predicted number of mutations, with power set at 0.80 and desired detectable difference of ±0.5 mutations. Among the 240 sequenced mutants from the six libraries (6x40), we found no bias towards a specific type of mutations (transitions vs. transversions), nor did we identify overrepresentation of any particular single point mutation or locus in this dataset. From the

sequenced mutants we could estimate the proportion of re-ligated wildtype plasmid, in which the mutated region was not inserted and instead the wildtype used as the cloning template re-ligated back (this is a common occurrence with any library created through standard restriction-digestion cloning techniques). By observing the frequency of wildtype genotypes in the sequenced *trans* libraries (which, due to the relatively large number of mutations should not contain any wildtype sequences), we estimate that <5% of each library is re-ligated with the wildtype insert (Fig.2 – Source Data 2). As this is a relatively small frequency to estimate precisely from sequencing 120 clones (3x40 *trans* library sequences), we do not account for it when considering the proportion of wildtype cells in each library. More importantly, this bias should be the same for all libraries and is therefore unlikely to alter our comparative analyses. Finally, among the 240 sequenced plasmids, we did not observe any that contained neither the mutated nor the wildtype insert, as all sequenced plasmids had an insert from cloning.

To make the whole system libraries, we removed through restriction digestion the mutated *cis*-element from each *cis* library and cloned it into the plasmid library already containing *trans*-element mutants with the corresponding mutation probability. Note that system libraries created in this way would likely have somewhat reduced diversity compared to either *cis* or *trans* libraries, as stochastically some mutants present in the component libraries would not find their way into the combined system library. By our design, this potential reduction in diversity would be equally biased towards *cis* and *trans* mutants, and ought not to be inflated for one component compared to the other.

In this study we set out to understand phenotypic effects of mutations and to connect the DMEs to the epistasis between the two components. To achieve this goal, we investigated

the DMEs in random mutant libraries, therefore without knowing the identity of the specific mutants. We did not characterize individual mutants, as drawing conclusion about the effects of specific mutations would require an unachievable high number of mutants to be analyzed. This was because the relatively large number of mutations introduced, in particular in the *trans*-element where each individual in the low mutation probability library contained on average 7 point mutations, meant that we covered a very large mutational space. As such, we would need to characterize an astronomical number of mutants to gain the statistical power necessary to discern the effects of individual mutations from the interactions between them. Marginal sampling of such a huge sequence space, which is the best we could achieve, would tell us nothing about how individual positions affect the overall DME.

Single-cell fluorescence measurements

In order to obtain the distributions of phenotypic effects of mutations in mutant libraries, we used flow cytometry/fluorescence activated cell sorting (FACS) to analyze expression levels of a yellow fluorescence protein. For all libraries, we measured gene expression levels both in the absence and in the presence of the transcription factor CI, determined by absence or presence of the inducer aTc, respectively. Throughout, we use $\log_{10}$ of expression level as our phenotype of interest. Mutant libraries, as well as the wildtype construct, were grown overnight in M9 minimal media supplemented by 1% casamino acids, 2% glucose, and 30μg/ml kanamycin, and either without or with 8 ng/ml aTc. From this point, the investigator was blinded with respect to the identity of each processed library. Overnight populations were diluted 100 times, grown for two hours, diluted a further 10 times and their fluorescence measured in a BD FACSAria^{tm} III cell sorter. Fluorescence of 500,000 cells was measured for each replicate of each library. Two independent replicates of each

mutant library and the monoclonal wildtype population in each of the two growth conditions were measured in the manner described above. All flow cytometry data was subsequently analyzed in FlowJo^{tm} version 10.0.8r1, and measurements with extreme FSC-A and SSC-A values were excluded from the analyses. The two replicate measurements of each library exhibited the same distributions of fluorescence phenotypes (tested by the K-S test) and were pooled together, to give a million counts for each library.

We verified that 1 million individual measurements, as well as the library diversity of at least 30,000 mutants, accurately described phenotypic distributions of possible mutations. To ensure that we are capturing a significant proportion of all possible phenotypic effects, we subsampled progressively smaller number of measurements (n = 500,000; n = 250,000; n = 100,000; n = 50,000) of *cis*- and *trans*-element mutant libraries, in each relevant environment (both absence and presence of CI for *cis*-element libraries, and only presence of CI for *trans*-element libraries). We quantified the difference between each subsampled dataset and the corresponding full dataset using a K-S test, and found that, by randomly subsampling each dataset 50 times, the distributions of phenotypes in subsamples were not statistically different from the distribution of the full dataset (Figure 2 – Figure Supplement 8).

Calculating entropy of a DME

Shannon entropy was used as an estimate of how uniform the distribution is across the whole range of possible phenotypes. The range of possible phenotypes was defined by the minimum and the maximum fluorescence measurement in the entire dataset, across all measured mutant library DMEs. Entropy was calculated as:

$$\square = -\sum_{k} P_k \log P_k + \log \Delta x$$

549 , where P_k is the frequency of fluorescence measurements in the k^{th} bin, and Δx is the width
550 of the bin, which was set to 0.05. In principle, values of entropy estimates depend on the bin
551 width, so we checked explicitly that our conclusions do not depend on this particular choice.
552 Error associated with each entropy measurement was calculated using standard
553 bootstrapping methods. We performed a nonparametric permutation test to assess if the
554 differences in entropy are significant.
555
556 *Estimating gene expression noise from flow cytometry measurements*
557 We randomly isolated 20 *cis*, 20 *trans*, and 20 system mutants, from each mutation
558 probability library, giving rise to 180 isolates. Power analysis (power.anova.test function in
559 R statistical package) indicated that 20 samples in each category were sufficient to detect
560 differences in gene expression noise of 2%, at significance level of 0.05 and power greater
561 than 0.9. In a flow cytometer, we measured gene expression levels in the presence of CI in
562 100,000 individual counts, for two replicates of each mutant isolate, as well as for the
563 wildtype. First, using a K-S test, we confirmed that the two replicate distributions for each
564 mutant were not significantly different. We combined the two replicate measurements, and
565 then randomly sampled without replacement 5,000 reads from this common pool ten times
566 (Fig.2 – Figure Supplement 4;5;6). Gene expression noise for each such sub-sample of
567 5,000 reads was estimated as the coefficient of variation, as done in other studies on gene
568 expression noise (Metzger *et al.* 2015). Note that the gene expression noise measured in this
569 manner comes from two sources – the heterogeneity of gene expression between individual
570 cells and the measurement error inherent in the flow cytometer. We assume that the
571 measurement error is constant between all mutants, so that possible changes in the
572 coefficient of variation would indicate a difference in the heterogeneity of gene expression
573 between genetically identical individuals. Using ANOVA (aov function in R statistical

574 software, version 3.4.1), we asked if there were differences in the noise of gene expression
575 between the 60 mutants of the same mutation probability, as well as between all 180 tested
576 mutants. We performed this test separately for the mutants that had no expression (that were
577 fully contained in the 'no expression' category), and for all other mutants. These two groups
578 were treated separately because the flow cytometry fluorescence measurement is not
579 responding to the same intracellular environment when the cell is producing a fluorescence
580 protein and when it is not. As such, estimates of gene expression noise in the two
581 categorically different types of intercellular environments are not directly comparable (Fig.2
582 – Source Data 1). Note that the tests carried out across all three mutation probabilities,
583 which included 95 mutants with no fluorescence and 85 mutants with fluorescence, found
584 no differences in gene expression noise. The probability of mutants with significantly
585 different noise existing in the library but not being detected at such sample sizes is less than
586 10^{-4} (calculated using experimentally-observed within and between group variance and at
587 power level of 0.9). For a library of 30,000 random mutants, this would mean that no more
588 than 10 system mutants could have different gene expression noise. For such a small
589 number of mutants to skew the observed system DMEs and lead to an increase in
590 intermediate phenotypes would be possible only if they were strongly overrepresented in the
591 library. This is unlikely the case, since all 180 isolated mutants had growth rates that were
592 comparable to the wildtype, and hence increase in noise would have to be hugely beneficial
593 on a very short time scale (around 10 generations).
594
595 *Naïve convolution of component distributions as the null model for additivity between*
596 *mutations*
597 Let us consider the effects of mutations, m_{cis} and m_{trans}, in two components of a system. As
598 our phenotype of interest is $\log_{10}$ of fluorescence level, we assume that, if two mutations are

independent, their effects are additive: $m_{expected} = m_{cis} + m_{trans}$. A deviation from this additive assumption is termed epistasis, so that: $\varepsilon = m_{observed} - m_{expected}$. Note that a deviation from an additive expectation in log is equivalent to a multiplicative prediction on the linear scale. When considering a library of mutants in two components, their effects are represented by corresponding DMEs, $f_{cis}(m)$ and $f_{trans}(m)$, where m is the 'true' effect of a random mutation on the wildtype, in the absence of experimental noise and measurement errors. If one could obtain 'true' DMEs for mutant libraries (in the absence of any type of noise or error), then the additive null expectation should follow a simple convolution of the two distributions: $f_{expected} = f_{cis} * f_{trans}$. Any deviation of the observed combined library DME ($f_{observed}$) from the $f_{expected}$ is indicative of epistasis.

In a realistic setting, experimental noise and instrumental error prevent direct measurements of the 'true' underlying DME (f), so that any measured DME (F) incorporates all the errors with its 'true' DME f. This means that, if the experimental noise and instrumental error do not change between mutants and across the dynamical measurement range, as is the case for our data (Fig.2 – Source Data 1; Fig.3 – Source Data 3), then the observed DME (F) of a mutant library is equivalent to a convolution between its 'true' underlying DME (f) and the measured wildtype distribution (F_{wt}): $F = f * F_{wt}$. In other words, the 'true' DME (f) shows how mutations alter wildtype expression. It follows that the additive prediction for the combined library, in the absence of epistasis, is a convolution of three DMEs:

$F^{+}_{expected} = f^{+}_{expected} * F^{+}_{wt} = f^{+}_{cis} * f^{+}_{trans} * F^{+}_{wt}$

,where f^{+}_{cis} and f^{+}_{trans} are the 'true' distributions of the *cis*- and the *trans*-element, respectively, and the superscript '+' indicates the presence of CI. The same equality would of course hold true in the absence of CI, but the analysis is trivial, as then the *trans* library shows no difference to the corresponding wildtype F^{--}_{wt}, i.e. f^{--}_{trans} is a unit element for the

operation of convolution (delta-distribution). For simplicity, we will omit the subscript when discussing DMEs obtained in the presence of CI.

The additive prediction (multiplicative in $\log_{10}$ of expression) can be rewritten in two equivalent forms:

(i) $F_{\text{expected}} = F_{\text{cis}} * f_{\text{trans}}$

(ii) $F_{\text{expected}} = f_{\text{cis}} * F_{\text{trans}}$

To obtain either of the underlying 'true' DMEs, we would need to deconvolve the wildtype distribution from one of the measured component library DMEs. However, although well understood and well behaved analytically, (de)convolutions are known to be highly unstable when used on numerical datasets, like ours. Therefore, we would need at least one of the component distributions in their analytical form. Instead of fitting one of the measured DMEs to some analytical representation followed by a deconvolution, we decided to directly 'reverse engineer' one of the component DMEs. We chose the *cis* DME in the presence of CI, as the simpler of the two. Concretely, we searched for f_{cis}, such that its convolution with F_{wt} matches the observed F_{cis} as closely as possible. We assumed f_{cis} to be from the gamma-family, as a relatively wide family of curves often used to describe DMEs (Fig.2 – Figure Supplement 9A). We optimized three parameters of the f_{cis}: shape, scale, and location, to minimize the squared differences between the observed *cis*-element DME (F_{cis}) and $f_{cis} * F_{\text{wt}}$ (Fig.2 – Figure Supplement 9B). Note that the 'true' *cis* DME indicates that effectively all mutations in *cis* are either neutral or they increase expression. Because of this, convolving the 'true' *cis* distribution with any other distribution results in an overall increased expression, independently of where the original distribution is centered. This is in line with the usual treatment of single mutant effects: if an effect of a mutation is positive,

the additive model states that the effect remains positive (and the same), independently of the genetic background.

After we obtained the 'true' DME for *cis* (f_{cis}), we convolve it with the observed *trans* DME to produce a naïve null-model for the system DME in the absence of epistasis. Convolving without any adjustments results in a part of the predicted system DME that lies beyond the highest experimentally recorded fluorescence levels (Fig.2 – Figure Supplement 9C). Because we use one of the strongest known promoters, the Lambda P_R, predictions that have higher expression than the wildtype are not biologically meaningful, as no combination of component mutations could experimentally result in such high expression levels. To reflect this maximal biologically obtainable limit to expression levels, we introduce a cutoff, effectively treating any mutant that would result in higher expression levels as having the wildtype expression. In practice, we (i*)* removed the high expression peak from the *trans* DME (as convolution with those mutants gives rise to higher expression levels), (ii*)* performed a convolution between the remainder of the *trans* DME and the f_{cis}, (iii*)* introduced a smooth cutoff at maximum expression levels to the convolved distribution, and (iv*)* added back the residual part of the high-expressing mutants. More specifically in the first step, we fitted the fraction α of the wildtype distribution in the absence of CI (F^{--}_{wt}) to minimize its (square) difference to the right-hand part of the high-expression *trans* peak (Fig.2 – Figure Supplement 9D, E). In this way we obtained a smooth remainder to convolve with f_{cis}, which will produce biologically realistic values. In the end, we add back the distribution of the wildtype in the absence of CI (F^{--}_{wt}), so to obtain a properly normalized predicted distribution (Fig.2 – Figure Supplement 9F). Because we impose this limit to the highest biologically obtainable expression level, convolving a hypothetical

distribution consisting of predominantly high expression phenotypes with the 'true' *cis* distribution (f_{cis}) would result in only high expression phenotypes.

The prediction for the system DME obtained in this manner reflects only two assumptions: the additive assumption of no epistasis, and the limit to maximal attainable expression levels. As such, this naïve prediction explicitly disregards any information about the genetic regulatory structure of the system. For each mutation probability, we evaluate if the predicted DME is different from the experimentally observed DME by conducting Pearson's Chi-squared test to compare the frequencies of mutants in the three expression categories ('no', 'intermediate', and 'high' expression).

Epistasis between random point mutants

We created 150 mutants with a random point mutation in *cis*, and 150 mutants with a random point mutation in *trans*. *Cis*-element mutants were identified by Sanger sequencing of 400 randomly selected mutants from the *cis*-element library with low (0.01) mutation probability. To obtain 150 *trans*-element mutants, we repeated the random mutagenesis protocol on *cI* with a very low mutation rate (yielding approximately 1 mutation per kb). From this reaction, we randomly selected and sequenced 500 mutants in order to identify 150 that contained only a single point mutation. Then, we created a library of 150 double mutants, with one point mutation in the *cis*- and the other in the *trans*-element. These 150 double mutants were unique, as each one consisted of a unique pairing between *cis* and *trans* point mutations, so that no point mutations were found in more than one double mutant (Fig.3 – Source Data 1).

In a plate reader, we measured fluorescence levels of all 150 double mutants as well as of their corresponding point mutants. The mutants, as well as the wildtype, were grown overnight in M9 minimal media supplemented with casamino acids, 30μg/ml kanamycin, and either in the absence of CI or in the presence of CI (induced with 8ng/ml of aTc). The overnight populations were diluted 1,000-fold, grown until OD_{600} of approximately 0.05, and their fluorescence measured in a Bio-Tek Synergy H1 platereader. This procedure was replicated six times for each mutant. We performed a series of pairwise t-tests in order to determine which isolates had significantly different fluorescence to the wildtype. Using a K-S test, we compared if the system double mutants had a higher frequency of intermediate phenotypes.

Consistent with convolution-based analyses, we consider expression level as the $\log_{10}$ of fluorescence, so that epistasis is defined as a deviation from an additive model, as $\boldsymbol{\varepsilon} = m_{system} - (m_{cis} + m_{trans})$, where m_{system} is the wildtype-relative fluorescence of a system double mutant, and m_{cis} and m_{trans} the wildtype-relative fluorescence of the two corresponding single mutants. Epistasis was calculated in the presence of CI, as in the absence of CI all *trans* mutants exhibited wildtype expression, and all system double mutants had the same expression as the *cis* mutant alone. In order to statistically determine which double mutants exhibited epistasis (i.e. ε not equal 1), we conducted a series of FDR-corrected *t*-tests. The errors were calculated based on six replicates, using error propagation to account for the variance due to normalization by the wildtype. Variance was not significantly different between measured mutants (Fig.3 - Source Data 2).

It is possible that the estimates of epistasis through population-level measures of fluorescence levels in a plate reader might not be equivalent to estimates obtained through

flow cytometry. This would particularly be true if the gene expression noise varied significantly between mutants. In order to confirm this is not the case in our study, we randomly selected 30 double mutants that, based on plate reader measurements, were in significant positive epistasis, 10 double mutants that were in significant negative epistasis, and 20 mutants that were not in significant epistasis. Then, we measured the fluorescence in 100,000 individual reads for two replicates of each isolate in a flow cytometer, in the absence and in the presence of CI (Fig.3 – Figure Supplement 3;4;5). First, we compared if gene expression noise between single and double mutants was the same, by conducing the same kind of analysis as described above, and found no differences between mutants (mutants with no expression: $F_{83,747} = 0.891$; P=0.59; mutants with expression: $F_{95,855} = 1.332$; P=0.174) (Fig.3 – Source Data 3). We also confirmed that the noise in single/double mutants was not different to the gene expression noise in isolates from low, intermediate, and high mutation probability libraries (mutants with no expression: $F_{166,1494} = 0.765$; P=0.746; mutants with expression: $F_{180,1620} = 1.385$; P=0.485). Then, we calculated epistasis in the presence of CI from flow cytometry measurements in the same manner as described for plate reader measurements (Fig.3 – Source Data 4). To evaluate the significance of calculated deviations from the additive expectation (epistasis), we use error propagation on the standard deviation obtained from the combined flow cytometry distributions of the two replicates, and not on the variance between means of replicate measurements (since the measured means for each isolated mutant were near identical between replicates). Linear regression between the estimates of epistasis from the two types of measurements shows that flow cytometry gives the same description of epistasis as the plate reader measurements ($F_{1,58} = 350.5$; P<0.0001) (Fig.3 – Figure Supplement 6).

Because all 150 double mutants were sequenced, we could test if epistasis was associated with the location of mutations. For the *trans*-element, we identified three locations: the N-terminus and the C-terminus domains, and the linker region between them (Fig.3 – Source Data 1). For the *cis*-element, the mutations could either be in one of the CI operator sites, in the RNAP contact residues (-10 and -35 regions), in the sites that have direct contact with both, or those that do not have direct contact with either protein (Fig.3 – Source Data 1). Then, we tested if existence of epistasis depended on the location of point mutations through a Pearson's Chi-squared test, which considered only the binary value for epistasis: either the presence of significant epistasis or its absence.

Experimentally accounting for the genetic regulatory structure of the system

We wanted to explore if accounting for the genetic regulatory structure of the studied system would improve our ability to predict the system DME from the DMEs of its components. To this end, we put together the low mutation probability *trans*-element (Fig.2E) and high mutation probability *cis*-element libraries (Fig.2 – Figure Supplement 1D) and measured the DME for this library in the manner described above. We put together these two libraries as they have approximately the same average number of mutations (7 for the *trans*- and 6 for the *cis*-element), allowing a comparison that is not influenced by the actual number of mutations in each of the two elements.

In order to experimentally predict the frequencies of phenotypes in each category of the low mutation *trans*-element + high mutation *cis*-element library, we partitioned the low mutation probability *trans*-element library in the presence, and high mutation probability *cis*-element library in the absence of CI. Using FACS, we partitioned each library into three bins, corresponding to the no expression, intermediate, and high expression phenotype

770 categories. We sorted a minimum of 500,000 individuals into each bin, and grew them
771 overnight in LB with 30μg/ml kanamycin. Using these populations, we obtained a measure
772 of sorting accuracy by obtaining a DME of each *trans*-element partition after overnight
773 growth. We isolated the plasmids from all six partitioned populations (three *cis* and three
774 *trans*), and cloned all possible combinations of *cis*- and *trans*-element partitions to make
775 nine new mutant libraries. We obtained a DME for each of these libraries, in the manner
776 described previously.
777
778 Then, we obtained a prediction for the frequency of phenotypes in each of the three
779 categories for the system mutant library consisting of low mutation probability *trans*- and
780 high mutation probability *cis*-elements. To do so, we weighted the frequencies of
781 phenotypes in each category of each partition combination library in Fig.5 by the frequency
782 of that partition in the original *trans*-element library (Fig.2E). For example, no expression
783 *trans* + no expression *cis* library yielded 93.4% of phenotypes in 'no expression' category,
784 and 6.6% of phenotypes in 'intermediate phenotype' category. These were weighted by
785 0.686, which is the frequency of phenotypes in no expression *trans*-element category from
786 which this particular partition combination library was derived (Fig.2E). All weighted
787 frequencies in the three categories – 'no expression phenotypes', 'intermediate phenotypes',
788 and 'high expression phenotypes' – across all nine partition combination DMEs were added
789 up to obtain a prediction for the distribution of phenotypes for the whole system library. As
790 a control that it is the presence of the *cis* mutants that leads to a more accurate prediction of
791 frequencies in the three categories, we used the frequencies of phenotypes based on sorting
792 accuracy. These two predicted distributions (experimental prediction based on partition
793 libraries and the prediction based on sorting accuracy) were compared to the actual
794 distributions using a Pearson's Chi-squared test.

795

796 *Mathematically accounting for the genetic regulatory structure of the system*

797 We tested if accounting for the genetic regulatory structure improved the naïve convolution-
798 based prediction of the system DME. Similar to the experimental approach, we incorporated
799 the knowledge of the effects of *cis* mutations in the absence of CI (F^{--}_{cis}). In addition to the
800 previous analysis, we assume that *trans* mutants showing high expression phenotypes
801 (namely, those mutants that have the same expression as the wildtype in the absence of CI)
802 are loss of function mutants that do not bind any *cis* mutants. To incorporate this
803 information into the convolution, we (i) removed the high expression peak from the *trans*
804 DME; (ii) performed a convolution between the remainder of the *trans* DME and the f_{cis},
805 (iii) introduced a cutoff, and then, (iv) instead of adding back the high expression wildtype
806 in the absence of CI (F^{--}_{wt}), we add the distribution of *cis* mutations in the absence of CI (F^{--}
807 $_{cis}$). This distribution is, as for the naïve convolution, added in proportion to the removed
808 high expression *trans* phenotypes to normalize the whole distribution. Then, we evaluated
809 the difference between the predicted DME and the observed system DME using a Pearson's
810 Chi-squared test, as previously described. We did this for the three system libraries shown
811 in Fig.2 and for the high mutation probability *cis* + low mutation probability *trans* library,
812 shown in Fig.4.

813

814 *Not all intermolecular epistasis arises from the genetic regulatory structure of the system*

815 While considering the effects of *cis* mutations on RNAP binding (and hence accounting for
816 the genetic regulatory structure of the system) explained much of intermolecular epistasis
817 we observed in system DMEs, we wanted to evaluate the extent to which other mechanisms
818 might be contributing to epistasis between the *cis*- and the *trans*-element. To this end, we
819 designed a library of 150 system double mutants, by combining point mutations in *cis*- and

trans-elements with specific phenotypes. Namely, we selected 150 *trans* mutants that exhibited full repression, and 150 *cis*-element mutants that exhibited high expression in the absence of CI (Fig.6 – Figure Supplement 1). The system double mutant library made in this manner corresponds to the partition combination shown in Fig.5G. Note that not all 150 double mutants had a unique point mutation in the *cis*-element, since we could not identify 150 mutations in *cis* that did not significantly affect expression levels in the absence of CI. Then, we measured fluorescence levels for all double mutants and their constitutive single mutants, and from those measurements calculated epistasis, in the same manner as described above. Finally, we tested if existence of epistasis depended on the location of point mutations (Fig.6 – Figure Supplement 2; Fig.6 – Source Data 2) with Pearson's Chi-squared test, as previously described.

References

Anderson D. W., McKeown A. N., Thornton J. W., 2015 Intermolecular Epistasis Shaped the Function and Evolution of an Ancient Transcription Factor and its DNA Binding Sites. Elife **4**: e07864.

Barton N. H., Partridge L., 2000 Limits to Natural Selection. Bioessays **22**: 1075–1084.

Bataillon T., Bailey S. F., 2014 Effects of New Mutations on Fitness: Insights from Models and Data (CW Fox and TA Mousseau, Eds.). Annals of the New York Academy of Sciences **1320**: 76–92.

Bershtein S., Segal M., Bekerman R., Tokuriki N., Tawfik D. S., 2006 Robustness–Epistasis Link Shapes the Fitness Landscape of a Randomly Drifting Protein. **444**: 929–932.

Breen M. S., Kemena C., Vlasov P. K., Notredame C., Kondrashov F. A., 2012 Epistasis as the Primary Factor in Molecular Evolution. **490**: 535–538.

Camps M., Herman A., Loh E., Loeb L. A., 2007 Genetic Constraints on Protein Evolution. Critical Reviews in Biochemistry and Molecular Biology **42**: 313–326.

Charlesworth D., Charlesworth B., Morgan M. T., 1995 The Pattern of Neutral Molecular Variation Under the Background Selection Model. Genetics **141**: 1619–1632.

de Visser J. A. G. M., Krug J., 2014 Empirical Fitness Landscapes and the Predictability of Evolution.

Nature Reviews Genetics **15**: 480–490.

Eyre-Walker A., Keightley P. D., 2007 The Distribution of Fitness Effects of New Mutations. Nat Rev Genet **8**: 610–618.

Fontana W., Buss L. W., 1994 “The Arrival of the Fittest”: Toward a Theory of Biological Organization. Bulletin of Mathematical Biology **56**: 1–64.

Fontana W., Schuster P., 1998 Continuity in Evolution: On the Nature of Transitions. Science **280**: 1451–1455.

Halligan D. L., Keightley P. D., 2009 Spontaneous Mutation Accumulation Studies in Evolutionary Genetics. Annu. Rev. Ecol. Evol. Syst. **40**: 151–172.

Jacquier H., Birgy A., Le Nagard H., Mechulam Y., Schmitt E., Glodt J., Bercot B., Petit E., Poulain J., Barnaud G., Gros P. A., Tenaillon O., 2013 Capturing the Mutational Landscape of the Beta-Lactamase TEM-1. Proceedings of the National Academy of Sciences **110**: 13067–13072.

Johnson A. D., Poteete A. R., Lauer G., Sauer R. T., Ackers G. K., Ptashne M., 1981 λ Repressor and cro - components of an Efficient Molecular Switch. **294**: 217–223.

Kinney J. B., Murugan A., Callan C. G. J., Cox E. C., 2010 Using Deep Sequencing to Characterize the Biophysical Mechanism of a Transcriptional Regulatory Sequence. PNAS **107**: 9158–9163.

Lagator M., Paixão T., Barton N. H., Bollback J. P., Guet C. C., 2017 On the Mechanistic Nature of Epistasis in a Canonical cis-Regulatory Element. Elife: e25192.

Lee M., Shen H., Burch C., Marron J. S., 2010 Direct Deconvolution Density Estimation of a Mixture Distribution Motivated by Mutation Effects Distribution. Journal of Nonparametric Statistics **22**: 1–22.

Lutz R., Bujard H., 1997 Independent and Tight Regulation of Transcriptional Units in *Escherichia coli* via the LacR/O, the TetR/O and AraC/I1-I2 Regulatory Elements. Nucleic Acids Research **25**: 1203–1210.

Lynch M., Hagner K., 2015 Evolutionary Meandering of Intermolecular Interactions Along the Drift Barrier. Proc Natl Acad Sci USA **112**: E30–E38.

Markiewicz P., Kleina L. G., Cruz C., Ehret S., Miller J. H., 1994 Genetic Studies of the *lac* Repressor XIV: Analysis of 4000 Altered *Escherichia coli lac* Repressors Reveals Essential and Non-essential residues, as well as “Spacers” which do not Require a Specific Sequence. Journal of Molecular Biology **240**: 421–433.

Metzger B. P. H., Yuan D. C., Gruber J. D., Duveau F., Wittkopp P. J., 2015 Selection on Noise Constrains Variation in a Eukaryotic Promoter. : 1–18.

Nagai T., Ibata K., Park E. S., Kubota M., Mikoshiba K., Miyawaki A., 2002 A Variant of Yellow Fluorescent Protein with Fast and Efficient Maturation for Cell-Biological Applications. Nature Biotechnology **20**: 87–90.

Orr A. H., 2003 The Distribution of Fitness Effects Among Beneficial Mutations. Genetics **163**: 1519–1526.

887 Otto S. P., Lenormand T., 2002 Resolving the paradox of sex and recombination. Nature Reviews
888 Genetics **3**: 252–261.

889 Pakula A. A., Young V. B., Sauer R. T., 1986 Bacteriophage Lambda *cro* Mutations: Effects on
890 Activity and Intracellular Degradation. PNAS **83**: 8829–8833.

891 Podgornaia A. I., Laub M. T., 2015 Pervasive Degeneracy and Epistasis in a Protein-Protein
892 interface. Science **347**: 673–677.

893 Poelwijk F. J., Tănase-Nicola S., Kiviet D. J., Tans S. J., 2011 Reciprocal Sign Epistasis is a Necessary
894 Condition for multi-Peaked Fitness Landscapes. Journal of Theoretical Biology **272**: 141–144.

895 Ptashne M., 2011 Principles of a Switch. Nat Chem Biol **7**: 484–487.

896 Salgado H., Peralta-Gil M., Gama-Castro S., Santos-Zavaleta A., Muñiz-Rascado L., García-Sotelo J.
897 S., Weiss V., Solano-Lira H., Martínez-Flores I., Medina-Rivera A., Salgado-Osorio G., Alquicira-
898 Hernández S., Alquicira-Hernández K., López-Fuentes A., Porrón-Sotelo L., Huerta A. M.,
899 Bonavides-Martínez C., Balderas-Martínez Y. I., Pannier L., Olvera M., Labastida A., Jiménez-
900 Jacinto V., Vega-Alvarado L., Del Moral-Chávez V., Hernández-Alvarez A., Morett E., Collado-
901 Vides J., 2013 RegulonDB v8.0: Omics Data Sets, Evolutionary Conservation, Regulatory
902 Phrases, Cross-Validated Gold Standards and More. Nucleic Acids Research **41**: D203–13.

903 Sarkisyan K. S., Bolotin D. A., Meer M. V., Usmanova D. R., Mishin A. S., Sharonov G. V., Ivankov D.
904 N., Bozhanova N. G., Baranov M. S., Soylemez O., Bogatyreva N. S., Vlasov P. K., Egorov E. S.,
905 Logacheva M. D., Kondrashov A. S., Chudakov D. M., Putintseva E. V., Mamedov I. Z., Tawfik D.
906 S., Lukyanov K. A., Kondrashov F. A., 2016 Local Fitness Landscape of the Green Fluorescent
907 Protein. **533**: 397–401.

908 Shultzaberger R. K., Maerkl S. J., Kirsch J. F., Eisen M. B., 2012 Probing the Informational and
909 Regulatory Plasticity of a Transcription Factor DNA–Binding Domain (HD Madhani, Ed.). PLoS
910 Genetics **8**: e1002614.

911 Soskine M., Tawfik D. S., 2010 Mutational Effects and the Evolution of New Protein Functions.
912 Nature Reviews Genetics **11**: 572–582.

913 Wagner A., 2011 Genotype Networks Shed Light on Evolutionary Constraints. Trends in Ecology
914 and Evolution **26**: 580–587.

915 Wang X., Minasov G., Shoichet B. K., 2002 Evolution of an Antibiotic Resistance Enzyme
916 Constrained by Stability and Activity Trade-offs. Journal of Molecular Biology **320**: 85–95.

917 Weinreich D. M., Delaney N. F., DePristo M. A., Hartl D., 2006 Darwinian Evolution Can Follow Only
918 Very Few Mutational Paths to Fitter Proteins. Science **312**: 111–114.

919 White M. A., Kwasnieski J. C., Myers C. A., Shen S. Q., Corbo J. C., Cohen B. A., 2016 A Simple
920 Grammar Defines Activating and Repressing *cis*-Regulatory Elements in Photoreceptors.
921 CellReports **17**: 1247–1254.

922 Whitlock M. C., Phillips P. C., Moore F. B.-G., Tonsor S. J., 1995 Multiple Fitness Peaks and
923 Epistasis. Annu. Rev. Ecol. Syst. **26**: 601–629.

924 Yun Y., Adesanya T. M. A., Mitra R. D., 2012 A Systematic Study of Gene Expression Variation at
925 Single-Nucleotide Resolution Reveals Widespread Regulatory Roles for uAUGs. Genome Res

22: 1089–1097.

Acknowledgments

We thank N. Barton, T. Bergmiller, A. Betancourt, K. Bod'ova, C. Igler, C. Nizak, T. Paixão, M. Pleska, D. Siekhaus, M. Steinrueck, and G. Tkačik for their invaluable comments on the manuscript. This work was supported by the People Programme (Marie Curie Actions) of the European Union's Seventh Framework Programme (FP7/2007-2013) under REA grant agreement n° [291734] to M.L. and European Research Council under the European Union's H2020 Programme (FP/2007-2013) / ERC Consolidator Grant [n. 648440] to J.P.B.

The authors declare no competing interests.

The data will be deposited in Dryad Digital Depository and PMC Plus upon acceptance of the manuscript for publication.

Figures and tables

effect of mutations in *cis* \ effect of mutations in *trans*	no expression	intermediate expression	high expression
no expression	no	intermediate	high
intermediate expression	intermediate	intermediate + high	high +
high expression	high	high +	high +

Table 1. Additive null predictions for interactions between mutations. Most interactions result in high expression phenotypes because the wildtype in the presence of CI has no expression, meaning that mutations are either neutral or increase wildtype expression. If an effect of a mutation is positive, the additive model states that the effect remains positive (and the same), independent of the genetic background. As such, these predictions are true only for a system that is tightly repressed, where the wildtype has no expression. 'High +' indicates predictions that result in expression levels above the biologically meaningful limit, which is defined by the unrepressed P_R promoter (shown in Fig.2A). We treat these predictions as high expression phenotypes. We consider three categorical single component effects ('no expression', 'intermediate expression', and 'high expression'), and show the categorical effect predicted by the additive null model for the system. We use categorical effects only to provide an intuition for what the additive model predicts - to obtain actual predictions of system DMEs, we use convolution (as explained in detail in Materials and Methods section *Naïve convolution of component distributions as the null model for additivity between mutations*).

	Actual system (mutations in *cis* and *trans*)	Experimental Prediction (based on partition libraries)	Convolution (no knowledge of genetic structure)	Convolution (accounting for *cis* effects in absence of CI)	Null prediction (based on sorting accuracy)
no expression phenotypes (%)	61.8	55.1	44.4	62.9	68.6
intermediate phenotypes (%)	31.9	31.1	21.5	26.6	9.7
high expression phenotypes (%)	6.3	13.8	34.1	10.5	21.7
$\chi^2_{(2)}$ compared to actual distribution		5.49	24.7	1.89	59.8
P value		0.064	10^{-6}	0.388	10^{-13}

Table 2. **Predicting the system DME is possible only when accounting for epistasis between components**. Four different predictions for the frequency of mutants in each partition (no expression, intermediate, and high expression phenotypes) were compared to

964 the actual system distribution, measured in the presence of CI, and consisting of the high
965 probability *cis* + low probability *trans* libraries (Fig.4). The experimental prediction based
966 on distributions of nine partition-combination DMEs (Fig.5) was obtained by weighting the
967 nine DMEs with the relative frequency of the original *trans* partition they were derived
968 from (from Fig.2E - no expression partitions were weighted by 0.686; novel phenotype
969 partitions by 0.097; high expression partitions by 0.217). One convolution of *cis*- and *trans*-
970 element DMEs was performed in the absence of any knowledge of the genetic regulatory
971 structure of the system (naïve convolution), and the other by accounting for the effects of
972 *cis* mutations in the absence of CI (Fig.2 – Figure Supplement 9). The null prediction tested
973 if the observed distributions could arise only from the imprecise sorting of the original
974 *trans* library partitions (Fig.4J,K,L). Only the experimental prediction based on partition-
975 combination libraries and the convolution that accounted for the genetic regulatory
976 structure could explain the epistatic interactions between mutants in *cis*- and *trans*-elements
977 (shown in orange).
978
979 **Figure 1. Genetic organization of the Lambda phage switch and the experimental**
980 **system.** A) The Lambda phage switch consists of two transcription factors - CI and Cro;
981 two promoters - a strong promoter P_R and a weak promoter P_{RM} (not shown); and three
982 operator sites - O_{R1}, O_{R2}, and O_{R3}. B) The experimental synthetic system, where *cro* was
983 substituted with the fluorescence marker gene (*venus-yfp*) under control of P_R. The P_{RM}
984 promoter was removed by the removal of parts of O_{R3}. Located 500bp away on the reverse
985 strand and separated by a terminator sequence is the *cI* gene under control of an inducible
986 P_{TET} promoter. CI, the *trans*-element, is 714bp; the *cis*-element is 84bp long. C) CI dimers
987 bind cooperatively to O_{R1} and O_{R2}, leading to repression of the P_R promoter.
988

Figure 2. **DMEs of the whole system are more evenly distributed than the individual component DMEs**. In the experimental system, CI acts as a tight repressor. The distributions of fluorescence are shown in the absence of CI (red) and in the presence of CI (blue). Each distribution was obtained by measuring fluorescence of two independent measurements of 500,000 cells by flow cytometry, which were then pooled together. The dashed lines separate three categories of phenotypes – 'no expression' phenotypes (corresponding to repressed wildtype); 'high expression' phenotypes (corresponding to the wildtype in the absence of CI); and 'intermediate' phenotypes. No expression and high expression categories are defined to include >99.9% of the wildtype fluorescence distribution in the presence and in the absence of CI, respectively. The Shannon entropy (*S*) is used to estimate how uniform each distribution is across the entire range of possible expression levels. The associated standard deviation (±) is given for each *S* value. Blue numbers are percentage of counts in each category in the presence of CI. Numbers in parentheses are percentage of counts excluding the estimated percentages of uniquely transformed individuals carrying the wildtype genotype (see Methods). The naïve additive convolution prediction for each system library and the associated predictions for the frequency of mutants in each category are shown in grey. Pearson's Chi-squared test was used to assess the difference between the observed and the convolution-predicted frequency of mutants in each category (low: $\chi^2_{(2)}=8.20$; $P<0.05$; intermediate: $\chi^2_{(2)}=32.26$; $P<0.0001$; and high mutation frequency library: $\chi^2_{(2)}=74.51$; $P<0.0001$). The distributions of the effects of mutations for the *cis*-element, the *trans*-element, and the whole system in the absence of CI are shown in Fig. 2 – Figure Supplement 1. Fig. 2 –Figure Supplement 2 shows distributions of the effects of 150 single point mutations in the *cis*- and the *trans*-element. Statistical significance of the differences in entropy values between the mutant libraries is shown in Fig. 2 – Figure Supplement 3. Flow cytometry measurements of 20

individual isolates from each library are shown in Fig. 2 – Figure Supplement 4,5,6, the analysis of which was used to demonstrate that gene expression noise is constant (Fig. 2 – Source Data 1). Convolutions for each mutation probability performed with the knowledge of the genetic regulatory structure of the system are shown in Fig. 2 – Figure Supplement 7, while Fig. 2 – Figure Supplement 9 provides an explanation of how convolutions were performed. The outcome of the test for how sensitive the shapes of distributions are to the number of sampled individuals is shown in Fig. 2 - Figure Supplement 8, while the confirmation that the mutagenesis protocol resulted in expected distributions of the number of mutations are shown in Fig. 2 – Source Data 2.

Figure 3. Epistasis in 150 random system double mutants. We created 150 double mutants with one unique random point mutation in the *cis*- and the other in the *trans*-element (Fig.3 – Figure Supplement 1; Fig.3 – Source Data 1). In a plate reader, we measured expression levels of monoclonal populations of each double mutant and its constitutive single mutants in the presence of CI. Epistasis was estimated as the deviation of the observed double mutant effect from the additive expectation based on single mutant effects (shown for each double mutant in Fig.3 – Figure Supplement 2). The grey bar indicates measurements that are not in significant epistasis. Double mutants above the "no epistasis" line are in positive epistasis (observed double mutant effect is greater than the additive expectation), and those below are in negative epistasis. Distributions of mutational effects for single *cis* and *trans* mutants, as well as for the double system mutants are shown in Fig.2 – Figure Supplement 2, while the data for epistasis calculations is shown in Fig.3 – Source Data 2. By measuring expression levels of 60 random double mutants (shown in orange) and their constitutive single mutants in the flow cytometer, we confirmed that estimates of epistasis using the plate reader correspond to those based on flow cytometry

measurements (Fig.3 – Figure Supplement 6; Source Data 3), and that the noise of expression is constant for all mutants (Fig.3 – Figure Supplement 3,4,5; Source Data 4).

Figure 4. Distribution of expression phenotypes for the system with high mutation probability in the *cis*-element and low mutation probability in the *trans*-element. The distributions of fluorescence are shown in the absence of CI (shown in red) and in the presence of CI (shown in blue). Each distribution was obtained by pooling two independent measurements of 500,000 cells. The dashed lines separate three categories of phenotypes – no expression phenotypes (corresponding to repressed wildtype); intermediate expression phenotypes; and high expression phenotypes (corresponding to the wildtype in the absence of CI). Numbers are percentage of counts in each category, in the absence (red) and in the presence (blue) of CI. The naïve convolution-predicted DME in the presence of CI, performed in the absence of any knowledge of the genetic regulatory structure of the system, is shown in grey, together with the corresponding frequencies of mutants in each category. The convolution prediction that accounted for the regulatory structure is shown in dark green. Results of the Pearson's Chi-squared test for the differences between the observed and both types of convolution-predicted DMEs in the presence of CI are shown in Table 2.

Figure 5. **Understanding the interactions between mutations in *cis* and *trans* by accounting for the genetic regulatory structure of the system**. Three partitions, obtained by FACS, of the low mutation probability *trans*-element library (corresponding to no expression, intermediate, and high expression phenotypes) were combined with the three equivalent partitions of the high mutation probability *cis*-element library in the absence of CI. The *cis*-element library in the absence of CI shows only the effect of mutations on

RNAP binding. The DME of the original *trans*-element library, corresponding to Fig.2E, is shown on top. The DME of the original *cis*-element library, corresponding to Fig.2 – Figure Supplement 1D, is shown on the right. The arrows illustrate from which category of the original DME (either *trans* or *cis*) were the sorted mutants used to make the particular combined library. DMEs of all nine partition-combination libraries were estimated using flow cytometry, with each distribution obtained by pooling two independent measurements of 500,000 cells. Also shown is the sorting accuracy, obtained as the repeated DME measurement of each *trans* partition following the original FACS sorting (panels J,K,L). The distributions of fluorescence are shown in the presence of CI. The dashed lines separate three categories of phenotypes – 'no expression', 'intermediate', and 'high expression' phenotypes. Numbers are percentage of counts in each category. At least in part, intermolecular epistasis can be qualitatively explained by considering the genetic regulatory structure of the system, as follows. Panels A), B), and C): no expression *cis*-element mutants do not bind RNAP sufficiently to lead to expression, so that system mutants containing them remain in the 'no expression' bin irrespective of the effect of mutations in *trans*. D) no expression *trans*-element mutants fully repress on wildtype *cis*. When *cis*-element mutations of intermediate expression are introduced, some still bind the functional CI mutants leading to repression, while others carry mutations that prevent CI binding, resulting in intermediate expression system mutants. E) Intermediate expression CI mutants only partially repress on wildtype *cis*, but fully repress some *cis*-element mutants that have lowered RNAP binding. Other intermediate expression CI mutants do not bind a mutated *cis*-element background. F) High expression CI mutants cannot bind wildtype *cis*. Similarly, they do not bind intermediate expression *cis*-element mutants, resulting in intermediate expression in the system. G), H): Some high expression *cis*-element mutants can fully bind mutated but functional CI mutants, others can only partially

bind them, while some maintain full RNAP binding while losing all CI binding. I) non-functional CI mutants do not repress on wildtype *cis*, hence also not on mutated *cis*-element backgrounds.

Figure 6. Not all intermolecular epistasis can be explained by accounting for the underlying genetic regulatory structure of the system. We created 150 double mutants with single mutation combinations corresponding to Fig.5G. A double mutant in this library would not be in epistasis unless a mutation in *trans* binds the *cis* mutant differently than the wildtype *trans* does. In a plate reader, we measured expression levels of monoclonal populations of each double mutant and its constitutive single mutants in the presence of CI. Epistasis was estimated as the deviation of the observed double mutant effect from the additive expectation based on single mutant effects. The grey bar indicates measurements that are not in significant epistasis. The effects of single mutations in *cis* and in *trans*, as well as the double mutant effects, are shown in Fig.6 – Figure Supplement 1, while the underlying data is shown in Fig.6 – Source Data 1. The location of point mutations is shown in Fig.6 – Figure Supplement 2 and Fig.6 – Source Data 2.

Figure 2 – Figure Supplement 1. DMEs for *cis*-element, *trans*-element, and system libraries in the absence of CI. In the experimental system, CI acts as a tight repressor. Each distribution was obtained by measuring fluorescence of two independent measurements of 500,000 cells by flow cytometry, which were then pooled together. The dashed lines separate three categories of phenotypes. ‘No expression’ and ‘high expression’ categories are defined to include >99.9% of the wildtype fluorescence distribution in the presence and in the absence of CI, respectively. Red numbers are percentage of counts in each category in the absence of CI. Numbers in brackets are percentage of counts excluding

the estimated percentage of uniquely transformed individuals carrying the wildtype genotype. DMEs of the *trans*-element library in the absence of CI are the same as the wildtype. DMEs of the *cis*-element and system libraries with equivalent mutation probability are not different from each other in the absence of CI.

Figure 2 – Figure Supplement 2. Distribution of single mutation effects in 150 random system double mutants and their corresponding single mutants. We created 150 random unique double mutants, with one point mutation in the *cis*- and the other in the *trans*-element. We measured gene expression of each mutant at a population level in a plate reader. Histogram of expression levels in the absence and in the presence of CI are shown for: A) point mutations in *cis*; B) point mutations in *trans*; C) double mutants in the system. Dotted line represents mean wildtype fluorescence in the corresponding environment. Six replicates of each mutant were measured. Grey bars indicate mutants that were not significantly different from the wildtype. The data underlying this figure is shown in Fig.3 – Source Data 2. The data from this library is used to calculate epistasis shown in Fig.3.

Figure 2 – Figure Supplement 3. Differences between calculated entropy estimates are statistically significant. P values of the differences in entropies of mutant libraries were calculated using a nonparametric permutation test.

Figure 2 – Figure Supplement 4. Mutant isolates from the low mutation probability libraries. 20 mutants were arbitrarily isolated from the *cis*, the *trans*, and the system library, and the expression of two replicates of each isolate in the presence of CI was measured for 100,000 individuals in the flow cytometer. From these measurements, we calculated the gene expression noise for each isolate (Fig.2 – Source Data 1). Each

histogram shows the combined distribution based on two replicate measurements, for each mutant isolate. The top histogram shows the monoclonal wildtype distribution in the absence (red) and in the presence (blue) of CI.

Figure 2 – Figure Supplement 5. Mutant isolates from the intermediate mutation probability libraries. 20 mutants were arbitrarily isolated from the *cis*, the *trans*, and the system library, and the expression of two replicates of each isolate in the presence of CI was measured for 100,000 individuals in the flow cytometer. From these measurements, we calculated the gene expression noise for each isolate (Fig.2 – Source Data 1). Each histogram shows the combined distribution based on two replicate measurements, for each mutant isolate. The top histogram shows the monoclonal wildtype distribution in the absence (red) and in the presence (blue) of CI.

Figure 2 – Figure Supplement 6. Mutant isolates from the high mutation probability libraries. 20 mutants were arbitrarily isolated from the *cis*, the *trans*, and the system library, and the expression of two replicates of each isolate in the presence of CI was measured for 100,000 individuals in the flow cytometer. From these measurements, we calculated the gene expression noise for each isolate (Fig.2 – Source Data 1). Each histogram shows the combined distribution based on two replicate measurements, for each mutant isolate. The top histogram shows the monoclonal wildtype distribution in the absence (red) and in the presence (blue) of CI.

Figure 2 – Figure Supplement 7. Mathematical predictions that account for the genetic regulatory structure accurately describe the system DME. A) Distribution of the monoclonal wildtype population in the absence (red) and in the presence of CI (blue).

B) Low, C) Intermediate, and D) High mutation probability system mutant libraries. Shown in green are the convolutions that accounted for the effects of *cis* mutations in the absence of CI (Fig.2 – Figure Supplement 1). Frequencies of mutants in the three categories ('no', 'intermediate', and 'high' expression phenotypes) for the observed system DME are shown in blue, while those from the convolution are shown in green. Pearson's Chi-squared statistic and the associated P-value used to test for the differences between the observed and the predicted frequencies of mutants in the three categories are shown for each mutations probability.

Figure 2 – Figure Supplement 8. Observed distributions accurately describe phenotypic distributions of possible mutations. Comparison of random subsamples of each dataset to the full dataset using K-S test shows that observed distributions are not sensitive to reductions in sample size or mutant library diversity. We take 50 random subsamples for each subsample size of each *cis*- and *trans*-element mutant library in each relevant environment (both absence and presence of CI for *cis*-element libraries, only presence of CI for *trans* -element libraries). D-statistic from the K-S test is used to estimate significance (P value).

Figure 2 – Figure Supplement 9. Predicting the system DME based on convolving component DMEs. We attempted to predict the DME for the system by convolving the corresponding DMEs of *cis* and *trans* components. To do this, we convolved the 'true' *cis* distribution (f_{cis}) with the observed *trans* distribution (F_{trans}). Here, we use low mutation probability *trans* and high mutation probability *cis* libraries to illustrate the procedure. A) The 'reverse engineered' true *cis* distribution (f_{cis}), shows how the mutations in the *cis*-element alter wildtype expression levels. B) The specific f_{cis} was chosen so to minimize the

difference between the observed *cis*-element DME and the convolution between f_{cis} and the observed wildtype distribution in the presence of CI (F^{+}_{wt}). C) Convolving f_{cis} with unmodified F_{trans} gives a predicted system DME with values outside the biologically meaningful range. D) In order to impose a biological limit to high expression, which is given by the wildtype expression in the absence of CI, we removed the high expression peak in the observed *trans* DME. This was done by fitting a fraction of the wildtype distribution in the absence of CI (α) to minimize its (square) difference to the right-hand part of the high-expression *trans* peak (red shaded area). E) Modified *trans* DME after removing high expression phenotypes. F) The naïve convolution prediction for the system DME is obtained by convolving f_{cis} with the modified *trans* DME, and then adding back a corresponding amount of the high-expression wildtype distribution in the absence of CI. When convolving with the knowledge of the underlying genetic regulatory structure, we add back the *cis* DME in the absence of CI (modified by the scaling factor α). Here, the 'naïve' prediction is shown.

Figure 3 – Figure Supplement 1. Identity and location of mutations in the 150 random double mutant library. A) DNA sequence of the *trans*-element showing the N-Terminal Domain (red), C-Terminal Domain (blue), and the linker region connecting the two domains (black). B) DNA sequence of the *cis*-element showing the -35 and -10 RNAP recognition sites (from left to right, underlined), and the two CI repressor operators (green). Every point mutation in *cis* was randomly paired with each mutation in *trans*, to give rise to 150 unique double mutants.

Figure 3 – Figure Supplement 2. Single mutant effects, as well as predicted and observed double mutant effects. Bar charts show $\log_{10}$ of wildtype-normalized expression

levels for (i) measured single mutant effect in the *cis*- (blue) and (ii) in the *trans*-element (orange); (iii) predicted double system mutant expression based on single mutant effects (green), and (iv) observed double system mutant effect, for each double mutant. Numbers above the bar charts indicate double mutant identity, which correspond to Figure 3 – Source Data 1. Dashed line indicates same expression as the wildtype.

Figure 3 – Figure Supplement 3. 30 double mutants with their corresponding single mutants, which are in significant positive epistasis. From the library of 150 mutants shown in Fig.3, 30 double mutants that were in significant positive epistasis were randomly selected. Expression levels of two replicates of each double mutant, as well as its corresponding single mutants, in the absence and in the presence of CI were measured for 100,000 individuals in the flow cytometer. Each panel shows the combined distribution based on two replicate measurements, for each mutant, in the absence (red) and in the presence (blue) of CI. From these measurements, we calculated gene expression noise for each isolate (Fig.3 – Source Data 3), as well as epistasis (Fig.3 – Figure Supplement 2; Fig.3 – Source Data 4). The top histogram shows the monoclonal wildtype distribution in the absence (red) and in the presence (blue) of CI.

Figure 3 – Figure Supplement 4. 10 double mutants with their corresponding single mutants, which are in significant negative epistasis. From the library of 150 mutants shown in Fig.3, 10 double mutants that were in significant negative epistasis were randomly selected. Expression levels of two replicates of each double mutant, as well as its corresponding single mutants, in the absence and in the presence of CI were measured for 100,000 individuals in the flow cytometer. Each panel shows the combined distribution based on two replicate measurements, for each mutant, in the absence (red) and in the

presence (blue) of CI. From these measurements, we calculated gene expression noise for each isolate (Fig.3 – Source Data 3), as well as epistasis (Fig.3 – Figure Supplement 2; Fig.3 – Source Data 4). The top histogram shows the monoclonal wildtype distribution in the absence (red) and in the presence (blue) of CI.

Figure 3 – Figure Supplement 5. 20 double mutants with their corresponding single mutants, which are not in significant epistasis. From the library of 150 mutants shown in Fig.3, 20 double mutants that were not in significant epistasis were randomly selected. Expression levels of two replicates of each double mutant, as well as its corresponding single mutants, in the absence and in the presence of CI were measured for 100,000 individuals in the flow cytometer. Each panel shows the combined distribution based on two replicate measurements, for each mutant, in the absence (red) and in the presence (blue) of CI. From these measurements, we calculated gene expression noise for each isolate (Fig.3 – Source Data 3), as well as epistasis (Fig.3 – Figure Supplement 2; Fig.3 – Source Data 4). The top histogram shows the monoclonal wildtype distribution in the absence (red) and in the presence (blue) of CI.

Figure 3 – Figure Supplement 6. Flow cytometer and plate reader measurements give equivalent estimates of epistasis. Epistasis was calculated as the deviation of the double mutant effect from the additive prediction based on single mutant effects. From the original 150 double mutants measured in the plate reader, 30 that were in significant positive, 10 in significant negative, and 20 that were not in significant epistasis were selected (shown in orange in Fig.3). Epistasis for these 60 mutants was calculated based on mean fluorescence and standard deviation (gene expression noise) obtained through flow cytometry measurements of 200,000 individuals (Fig.3 – Figure Supplement 3;4;5). Linear regression

was performed to test for correlation between two experimental approaches to calculating epistasis. Dotted lines are the 95% confidence intervals around the no-epistasis null model (Log_{10}(epistasis) = 0). Grey areas indicate that the two experimental methods give the same qualitative description of epistasis (positive, negative, or no significant epistasis). The data underlying this figure is shown in Fig.3 – Source Data 2;4.

Figure 6 – Figure Supplement 1. Distribution of single mutation effects in 150 system double mutants and their corresponding single mutants. We created 150 unique double mutants, with one point mutation in *cis* that had high expression in the absence of CI, and the other in *trans* that exhibited no expression in the presence of CI. We measured gene expression of each mutant at a population level in a plate reader. Histograms of expression levels in the absence and in the presence of CI are shown for: A) point mutations in *cis*; B) point mutations in *trans*; C) double mutants in the system. Dotted line represents mean wildtype fluorescence in the corresponding environment. Six replicates of each mutant were measured. Grey bars indicate mutants that were not significantly different from the wildtype. The data underlying this figure is shown in Fig.6 – Source Data 1.

Figure 6 – Figure Supplement 2. Identity and location of mutations in the double mutant library with a *trans* mutation that has no expression in the presence of CI, and a *cis* mutation with high expression in the absence of CI. A) DNA sequence of the *trans*-element showing the N-Terminal Domain (red), C-Terminal Domain (blue), and the linker region connecting the two domains (black). B) DNA sequence of the *cis*-element showing the -35 and -10 RNAP recognition sites (from left to right, underlined), and the two CI repressor operators (green). Unlike the double mutant library shown in Fig.3, where each double mutant had a unique mutation in *cis* and *trans*, in this library some *cis*

mutations had to be repeated, as we could not identify 150 mutations in *cis* that had high expression in the absence of CI.

Figure 2 – Source Data 1. Gene expression noise is constant. The flow cytometry data obtained for 20 *cis*, *trans*, and system mutant isolates from each mutation probability library was used to quantify gene expression noise. The data provided here are shown in Fig.2 – Figure Supplement 4,5,6.

Figure 2 – Source Data 2. Sequencing 40 isolates from each *cis*- and *trans*-element library confirms the predicted distribution of the number of mutations. This data also allowed us to estimate the frequency of 'back' cloning (wildtype re-ligating instead of the desired insert), and of the frequency of 'failed' cloning (no insert of any type).

Figure 3 – Source Data 1. Identity and location of mutations in the 150 random double mutant library.

Figure 3 – Source Data 2. Calculating epistasis from the effects of 150 random double mutants and their corresponding single point mutations, measured in plate reader. The data provided here are shown in Fig.3, Fig. 2 – Figure Supplement 2, and Fig.3 – Figure Supplement 1.

Figure 3 – Source Data 3. Gene expression noise in single and double mutants is constant. Flow cytometry data obtained for 60 double mutants and their corresponding

single mutants, in the absence and in the presence of CI, was used to quantify gene expression noise. The data provided here are shown in Fig.3 – Figure Supplement 2,3,4.

Figure 3 – Source Data 4. Calculating epistasis from the effects of 60 random double mutants and their corresponding single point mutations, measured in flow cytometer. The data provided here are shown in Fig.3 – Figure Supplement 1.

Figure 6 – Source Data 1. Calculating epistasis from the effects of 150 double mutants and their corresponding single point mutations, measured in plate reader. This library consists only of point mutants in *cis* that lead to high expression in the absence of CI, and point mutants in *trans* that result in no expression in the presence of CI. The data provided here are shown in Fig.6, and Fig. 6 – Figure Supplement 1.

Figure 6 – Source Data 2. Identity and location of mutations in the library of 150 double mutant, with a point mutation in *cis* that leads to high expression in the absence of CI, and a point mutation in *trans* that leads to no expression in the presence of CI.

FIGURE 1

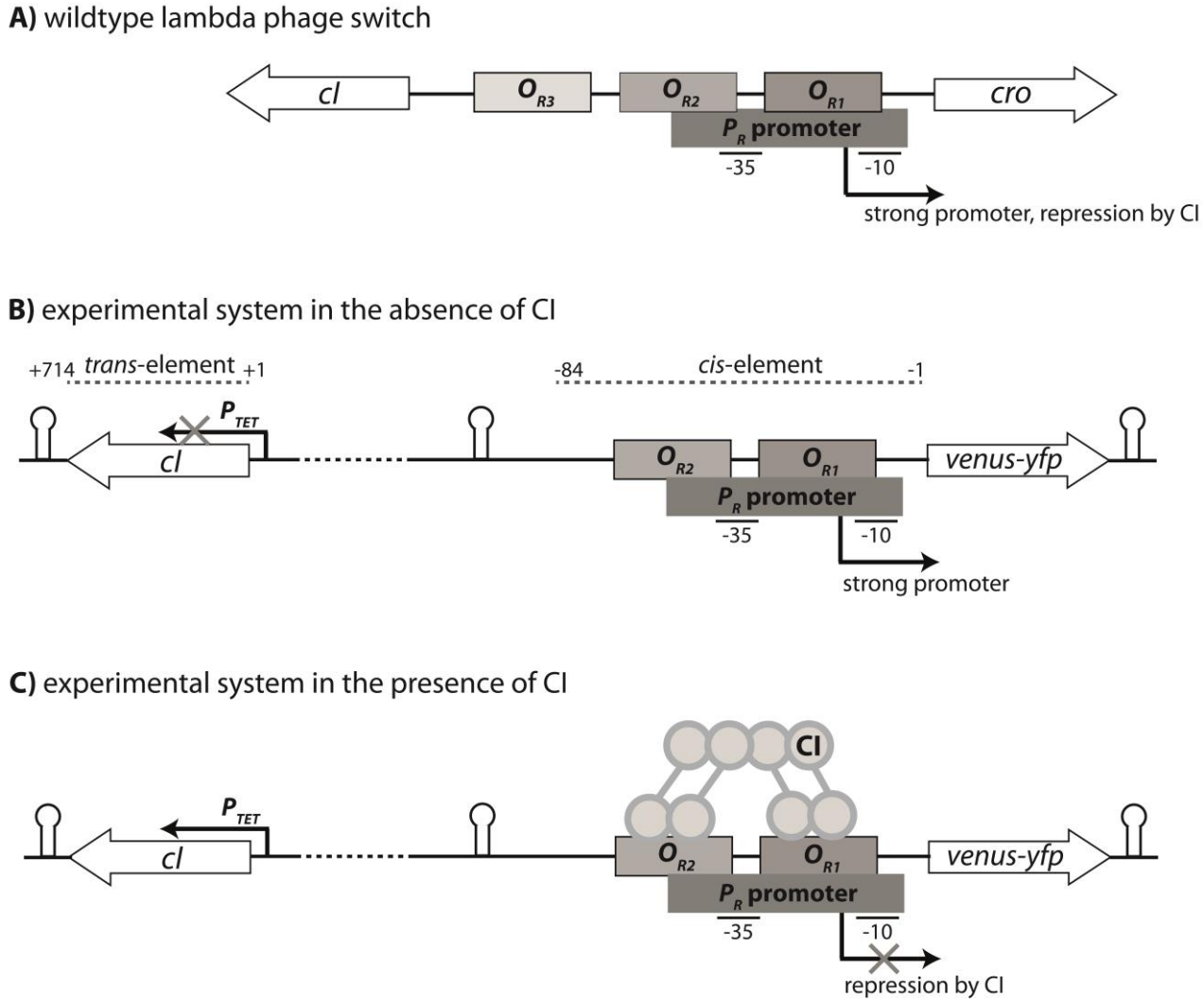
A) wildtype lambda phage switch
cI
O R3
O R2
O R1
cro
P R promoter
-35
-10
strong promoter, repression by CI
B) experimental system in the absence of CI
+714 trans-element +1
-84 cis-element -1
P TET
cI
O R2
O R1
venus-yfp
P R promoter
-35
-10
strong promoter
C) experimental system in the presence of CI
CI
P TET
cI
O R2
O R1
venus-yfp
P R promoter
-35
-10
repression by CI

FIGURE 2

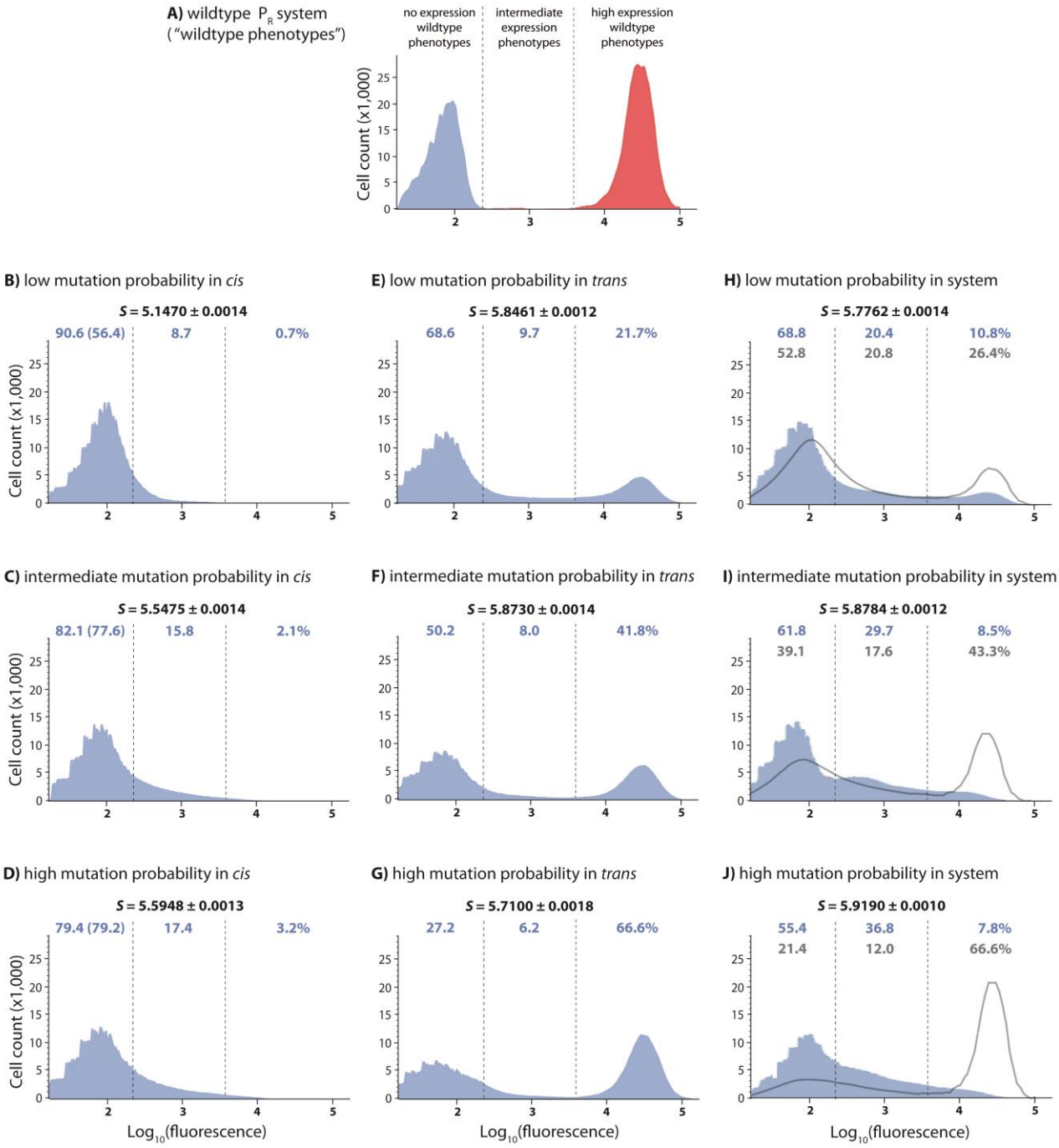
A) wildtype P_R system ("wildtype phenotypes")
no expression wildtype phenotypes
intermediate expression phenotypes
high expression wildtype phenotypes
Cell count (x1,000)
B) low mutation probability in cis
S = 5.1470 ± 0.0014
90.6 (56.4)
8.7
0.7%
C) intermediate mutation probability in cis
S = 5.5475 ± 0.0014
82.1 (77.6)
15.8
2.1%
D) high mutation probability in cis
S = 5.5948 ± 0.0013
79.4 (79.2)
17.4
3.2%
E) low mutation probability in trans
S = 5.8461 ± 0.0012
68.6
9.7
21.7%
F) intermediate mutation probability in trans
S = 5.8730 ± 0.0014
50.2
8.0
41.8%
G) high mutation probability in trans
S = 5.7100 ± 0.0018
27.2
6.2
66.6%
H) low mutation probability in system
S = 5.7762 ± 0.0014
68.8
20.4
10.8%
52.8
20.8
26.4%
I) intermediate mutation probability in system
S = 5.8784 ± 0.0012
61.8
29.7
8.5%
39.1
17.6
43.3%
J) high mutation probability in system
S = 5.9190 ± 0.0010
55.4
36.8
7.8%
21.4
12.0
66.6%
Log10(fluorescence)

FIGURE 3

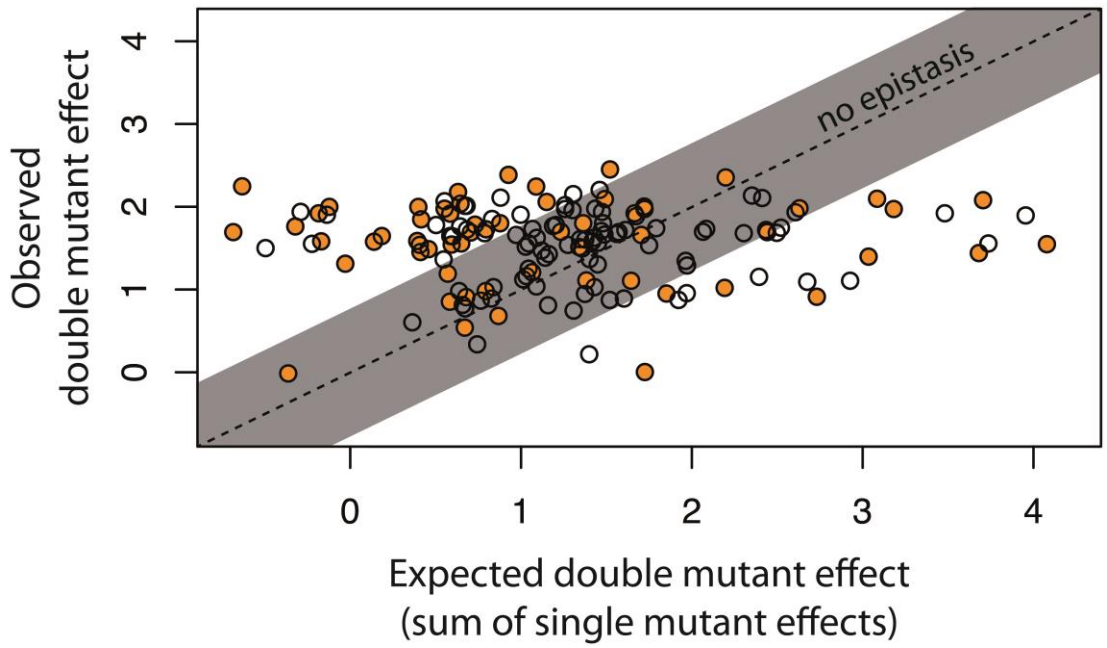
Observed
double mutant effect
0
1
2
3
4
no epistasis
0
1
2
3
4
Expected double mutant effect
(sum of single mutant effects)

FIGURE 4

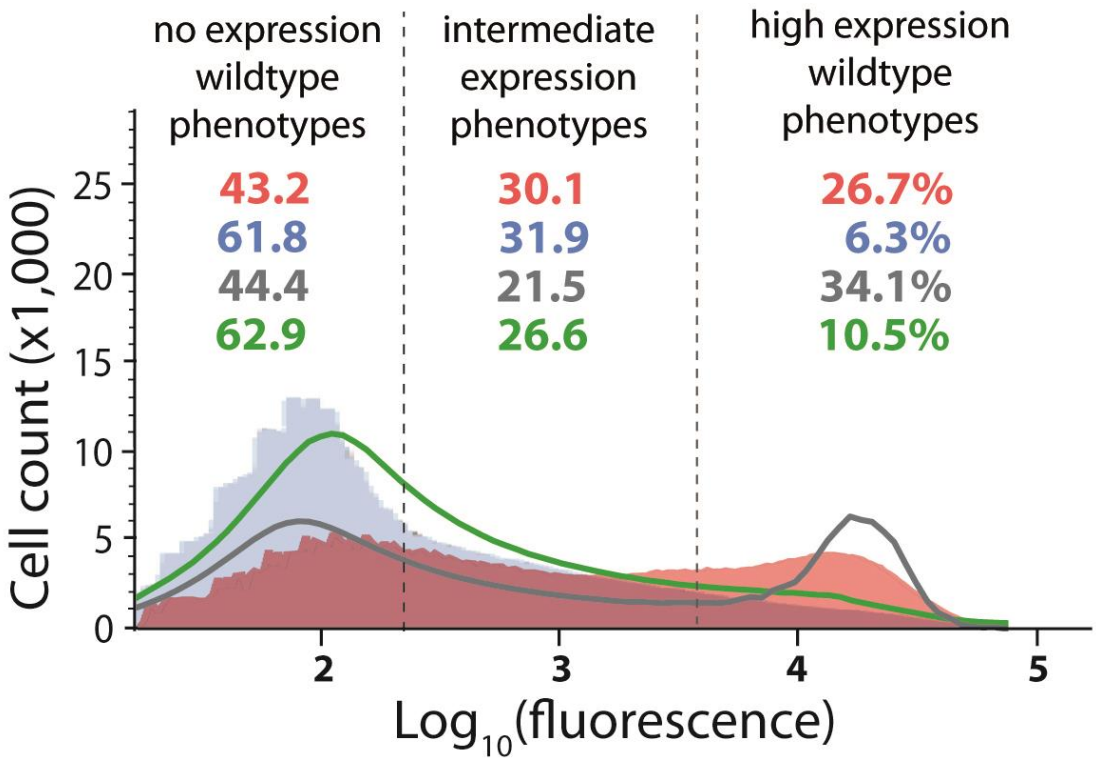
no expression wildtype phenotypes
intermediate expression phenotypes
high expression wildtype phenotypes
43.2
61.8
44.4
62.9
30.1
31.9
21.5
26.6
26.7%
6.3%
34.1%
10.5%
Cell count (x1,000)
25
20
15
10
5
0
2
3
4
5
Log10(fluorescence)

FIGURE 5

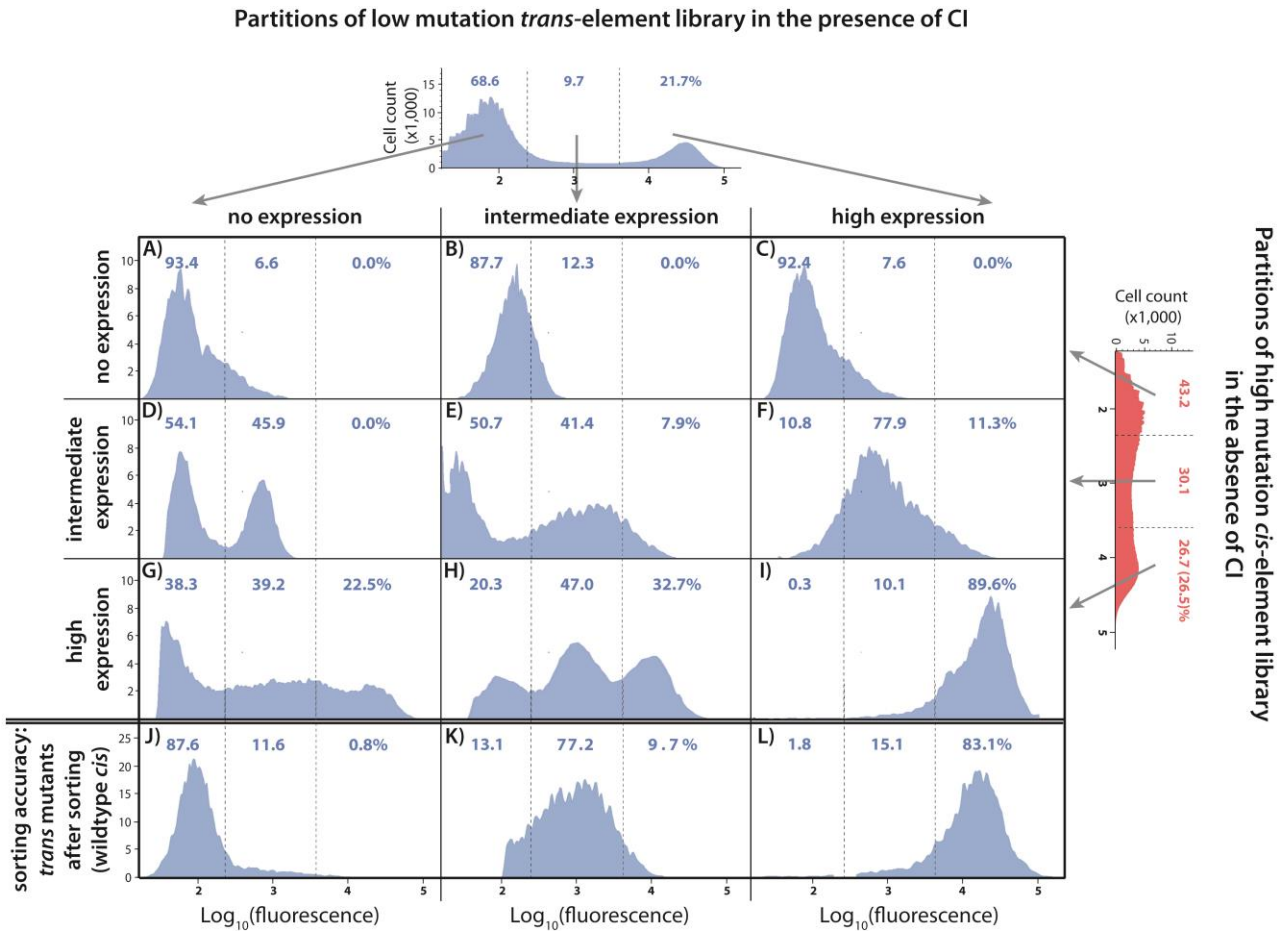
Partitions of low mutation *trans*-element library in the presence of CI
Cell count (x1,000)
68.6
9.7
21.7%
no expression
intermediate expression
high expression
A) 93.4 6.6 0.0%
B) 87.7 12.3 0.0%
C) 92.4 7.6 0.0%
D) 54.1 45.9 0.0%
E) 50.7 41.4 7.9%
F) 10.8 77.9 11.3%
G) 38.3 39.2 22.5%
H) 20.3 47.0 32.7%
I) 0.3 10.1 89.6%
J) 87.6 11.6 0.8%
K) 13.1 77.2 9.7%
L) 1.8 15.1 83.1%
sorting accuracy: *trans* mutants after sorting (wildtype *cis*)
Log10(fluorescence)
Cell count (x1,000)
43.2
30.1
26.7 (26.5)%
Partitions of high mutation *cis*-element library in the absence of CI

FIGURE 6

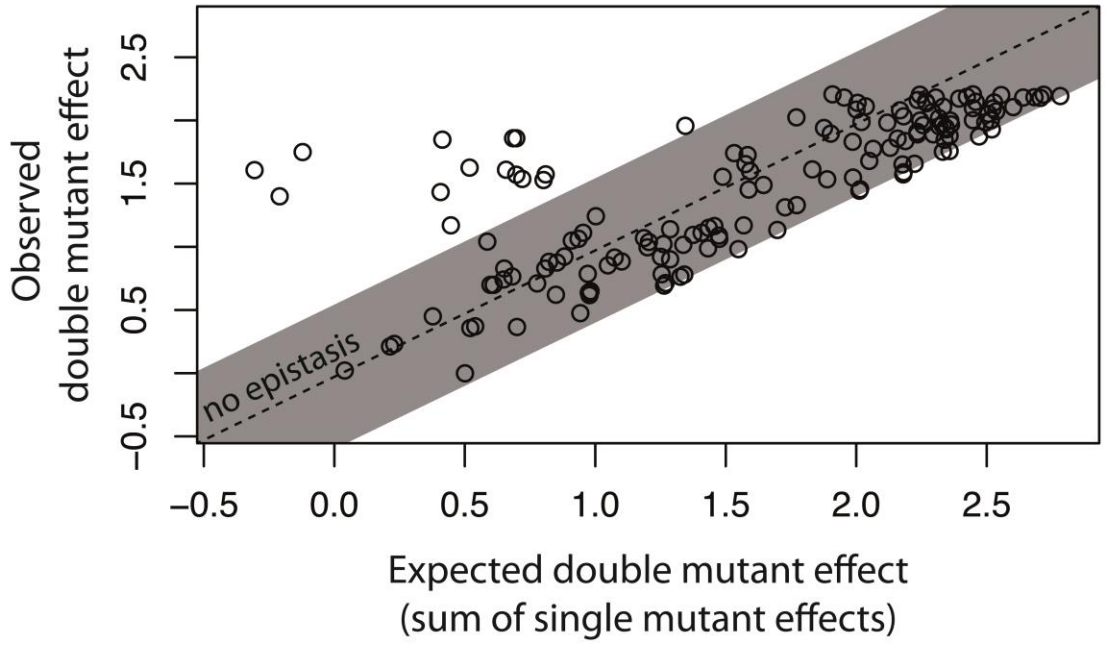
Observed
double mutant effect
2.5
1.5
0.5
−0.5
no epistasis
−0.5
0.0
0.5
1.0
1.5
2.0
2.5
Expected double mutant effect
(sum of single mutant effects)

Figure 2 – Figure Supplement 1

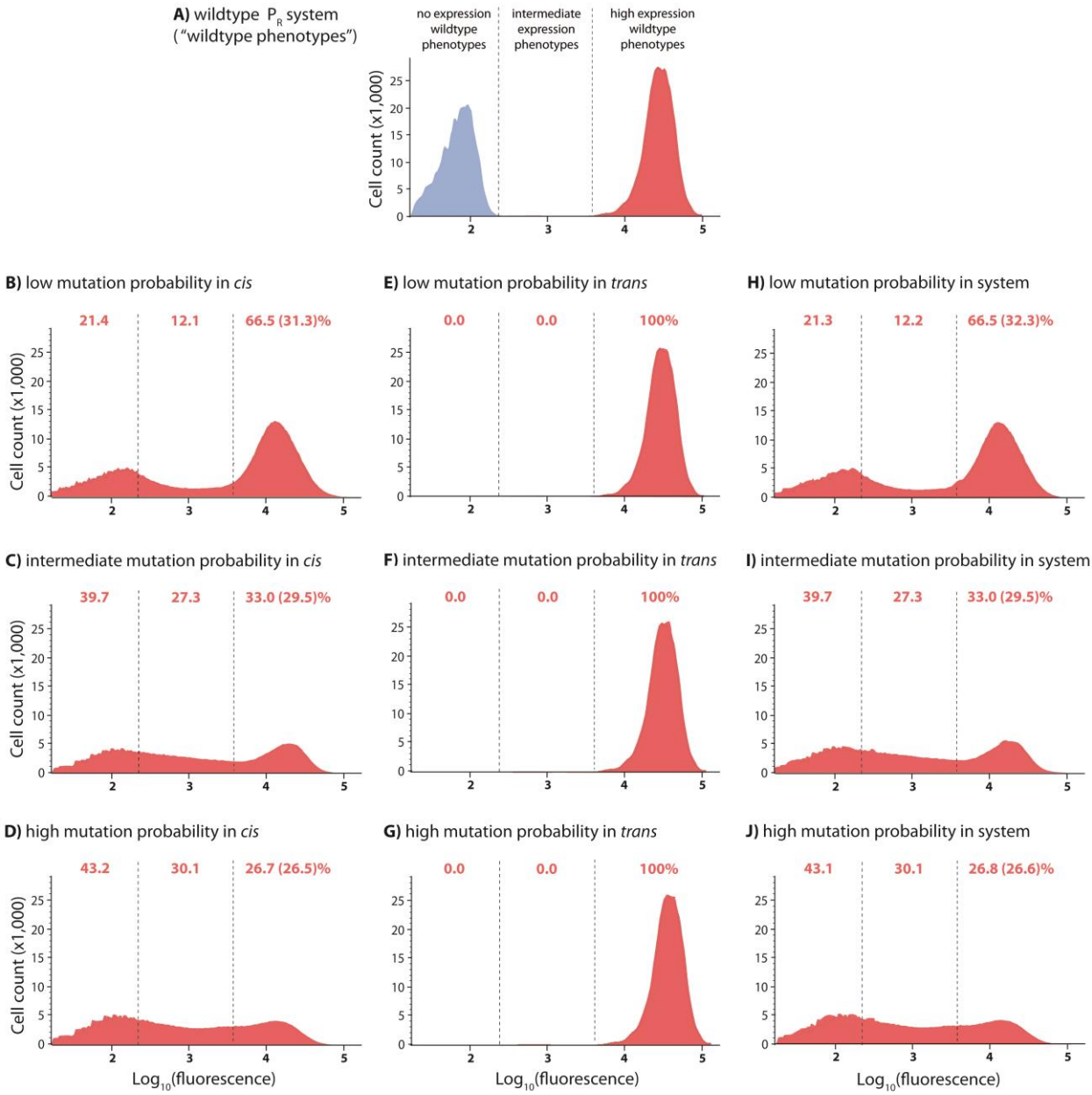

Figure 2 – Figure Supplement 2

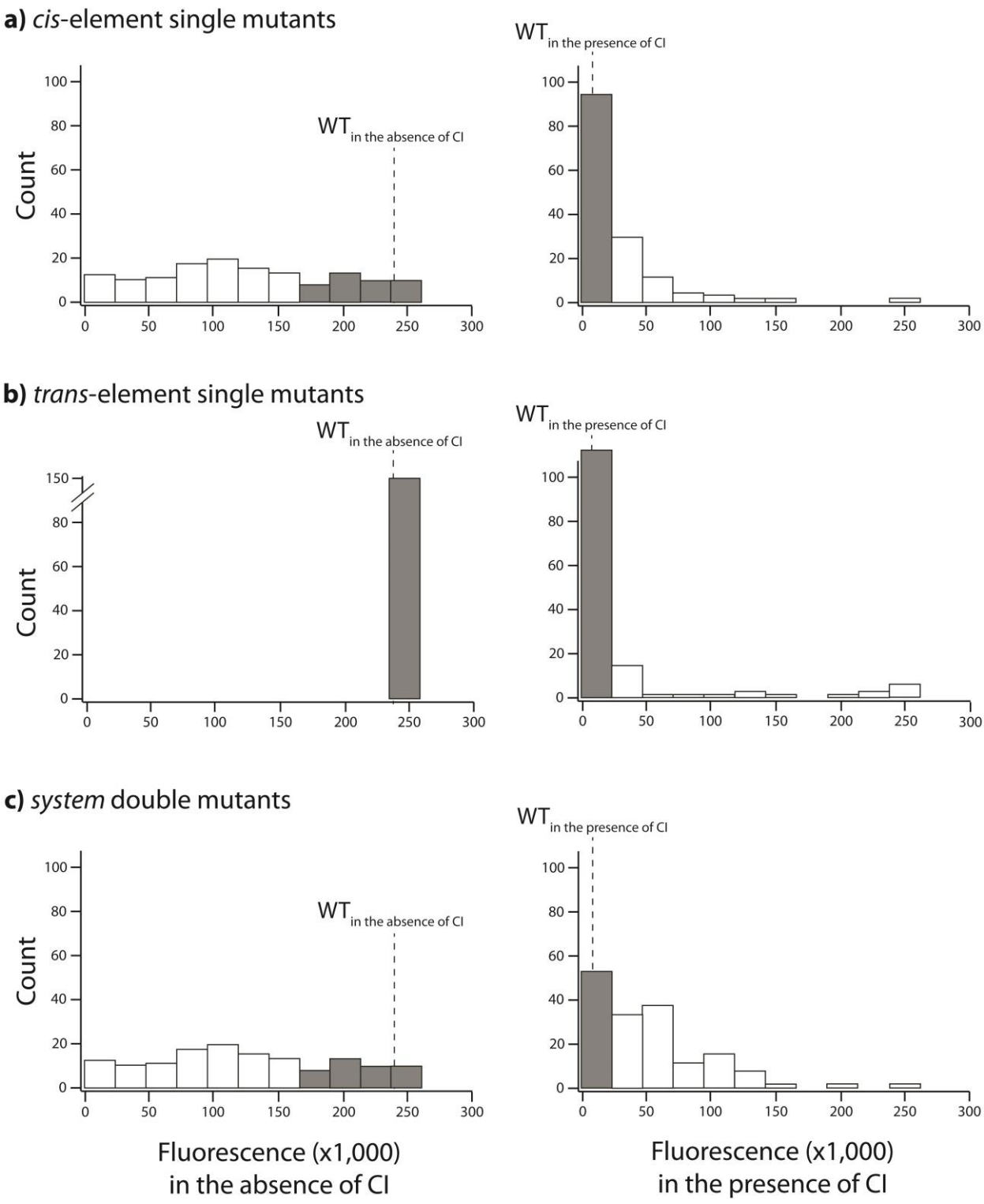

Figure 2 – Figure Supplement 3

	low mutation probability *cis*	intermediate mutation probability *cis*	high mutation probability *cis*	low mutation probability *trans*	intermediate mutation probability *trans*	high mutation probability *trans*	low mutation probability system	intermediate mutation probability system	high mutation probability system
low mutation probability *cis*		$< 10^{-6}$	$< 10^{-6}$	$< 10^{-6}$	$< 10^{-6}$	$< 10^{-6}$	$< 10^{-6}$	$< 10^{-6}$	$< 10^{-6}$
intermediate mutation probability *cis*			$< 10^{-6}$	$< 10^{-6}$	$< 10^{-6}$	$< 10^{-6}$	$< 10^{-6}$	$< 10^{-6}$	$< 10^{-6}$
high mutation probability *cis*				$< 10^{-6}$	$< 10^{-6}$	$< 10^{-6}$	$< 10^{-6}$	$< 10^{-6}$	$< 10^{-6}$
low mutation probability *trans*					$< 10^{-6}$	$< 10^{-6}$	$< 10^{-6}$	$< 10^{-6}$	$< 10^{-6}$
intermediate mutation probability *trans*						$< 10^{-6}$	$< 10^{-6}$	0.00239	$< 10^{-6}$
high mutation probability *trans*							$< 10^{-6}$	$< 10^{-6}$	$< 10^{-6}$
low mutation probability system								$< 10^{-6}$	$< 10^{-6}$
intermediate mutation probability system									$< 10^{-6}$
high mutation probability system									

Figure 2 – Figure Supplement 4

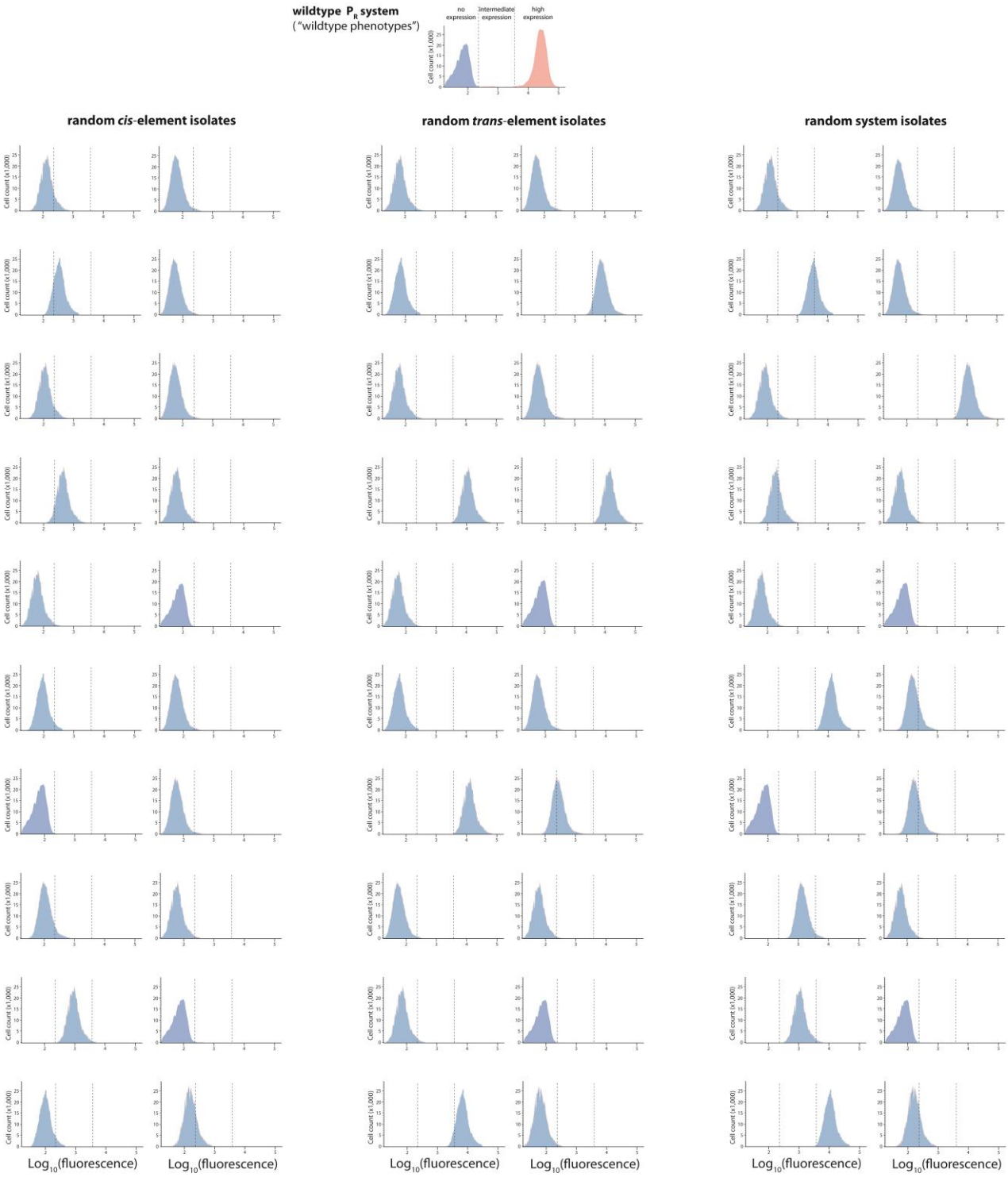

Figure 2 – Figure Supplement 5

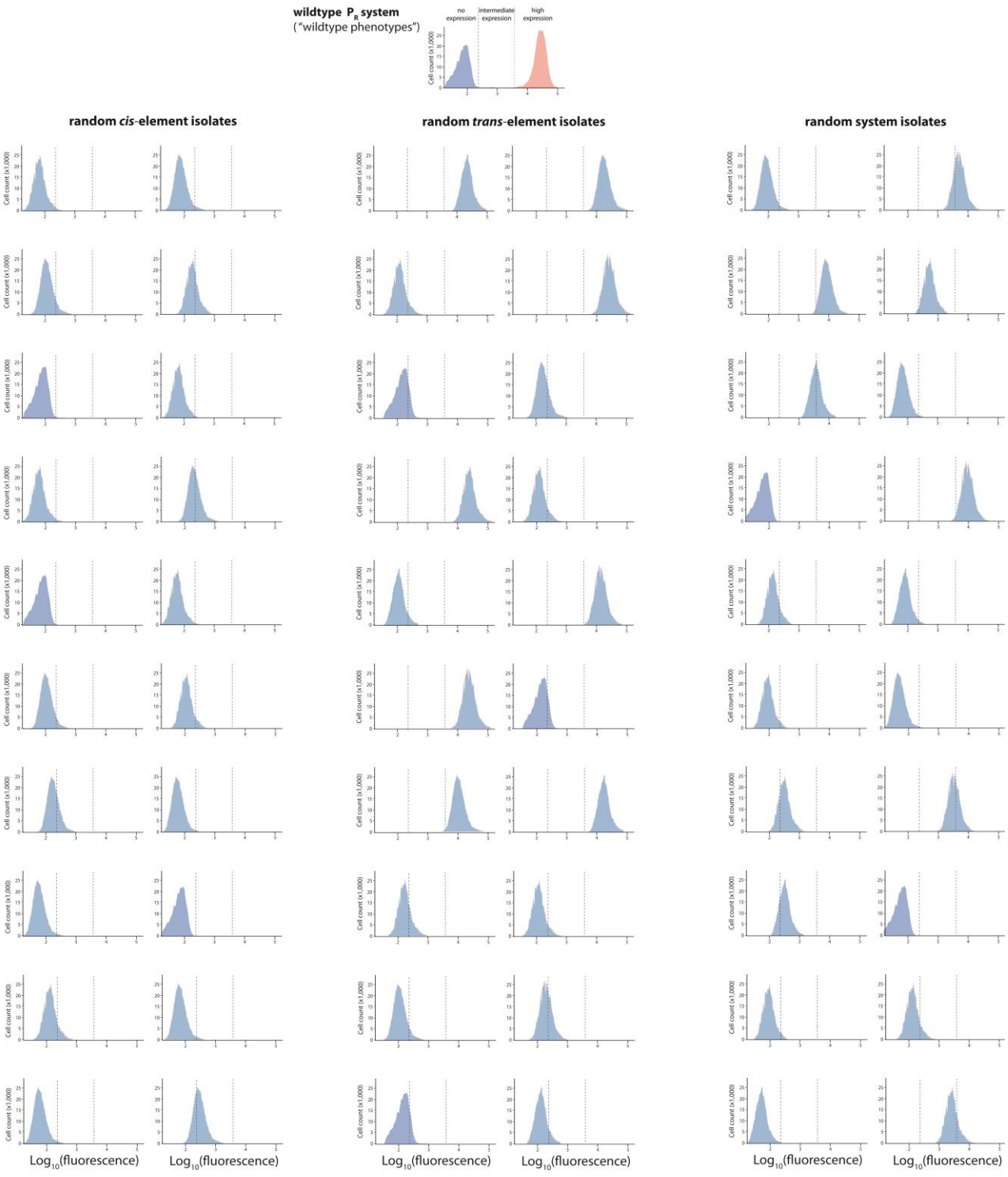

Figure 2 – Figure Supplement 6

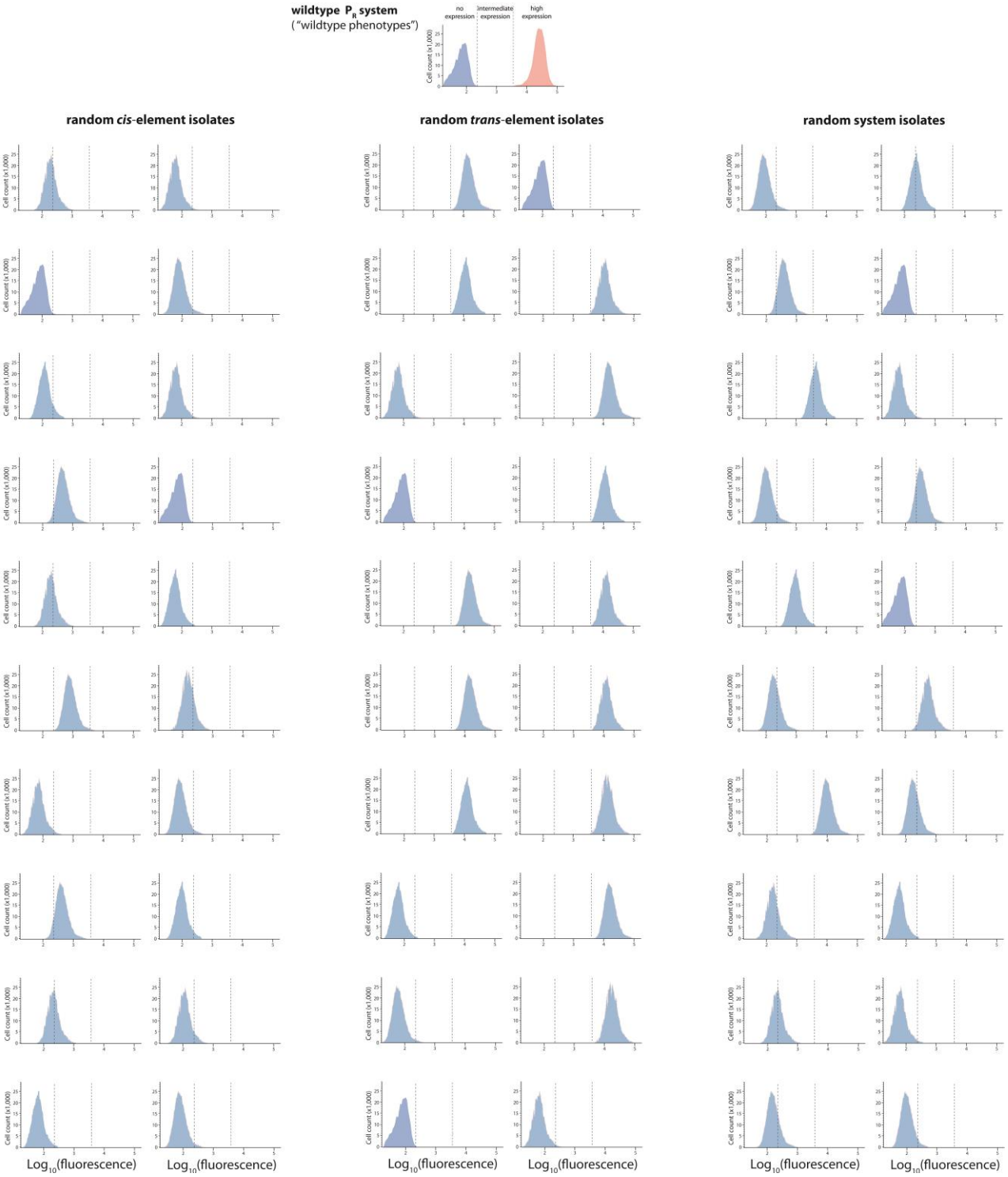

Figure 2 – Figure Supplement 7

A) wildtype P_R system ("wildtype phenotypes")

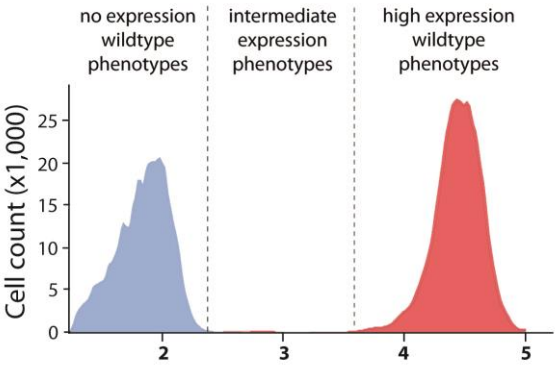

B) low number of mutations in system

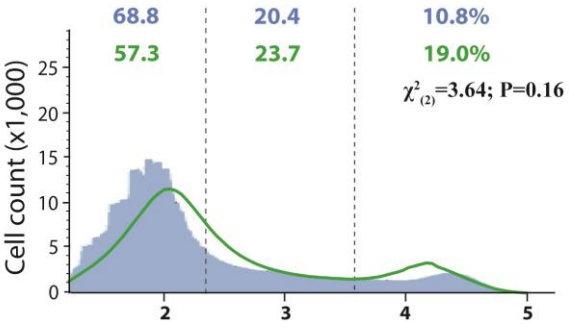

C) intermediate number of mutations in system

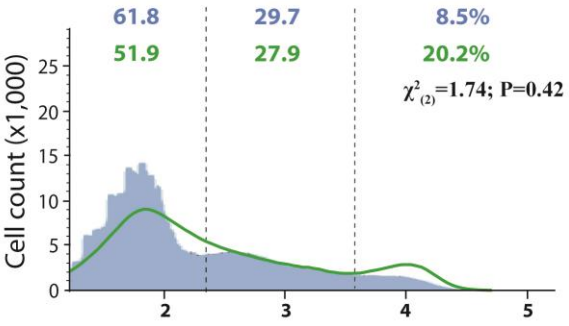

D) high number of mutations in system

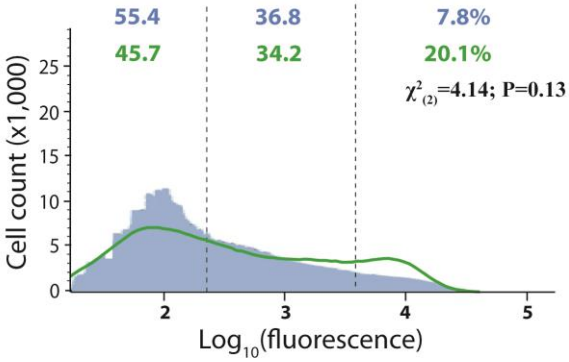

Figure 2 – Figure Supplement 8

Mutant library	Environment	Subsample size (x1,000)	D statistic	P value
Low mutation number *cis*	Absence of cI	50	0.0035	0.61
		100	0.0019	0.89
		250	0.0011	0.97
		500	$8x10^{-4}$	0.99
	Presence of cI	50	0.0026	0.90
		100	0.0024	0.70
		250	0.0012	0.94
		500	0.001	0.93
Intermediate mutation number *cis*	Absence of cI	50	0.0032	0.32
		100	0.0019	0.49
		250	0.0023	0.96
		500	$6x10^{-4}$	0.99
	Presence of cI	50	0.002	0.99
		100	0.0024	0.67
		250	0.0024	0.23
		500	$6x10^{-4}$	0.99
High mutation number *cis*	Absence of cI	50	0.0028	0.84
		100	0.0045	0.56
		250	0.001	0.99
		500	$6x10^{-4}$	0.99
	Presence of cI	50	0.0031	0.75
		100	0.0027	0.52
		250	0.001	0.99
		500	$9x10^{-4}$	0.96
Low mutation number *trans*	Presence of cI	50	0.0049	0.21
		100	0.0027	0.52
		250	0.0027	0.12
		500	$7x10^{-4}$	0.99
Intermediate mutation number *trans*	Presence of cI	50	0.0034	0.66
		100	0.0017	0.96
		250	0.0015	0.75
		500	$9x10^{-4}$	0.97
High mutation number *trans*	Presence of cI	50	0.0026	0.91
		100	0.0025	0.65
		250	0.002	0.41
		500	$6x10^{-4}$	0.99

Figure 2 – Figure Supplement 9

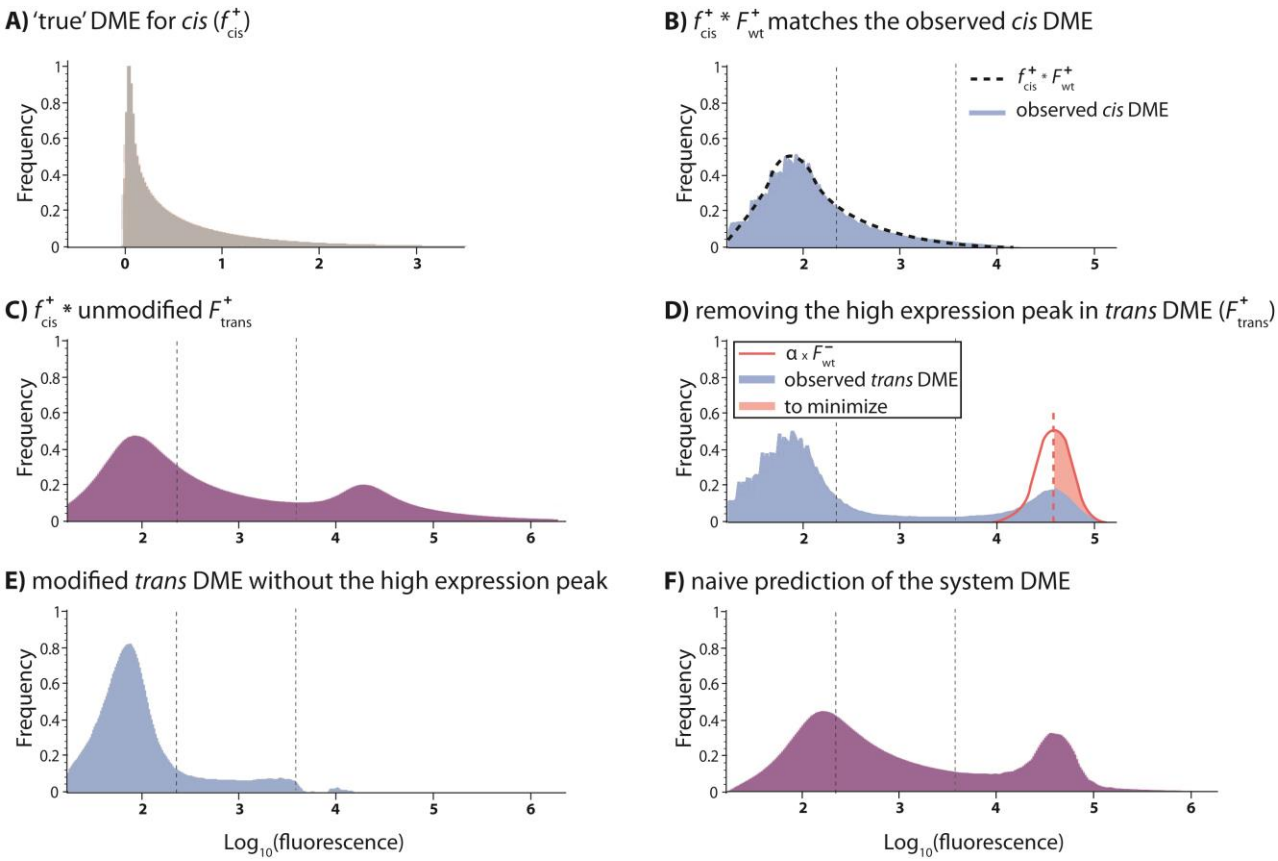

Figure 3 – Figure Supplement 1

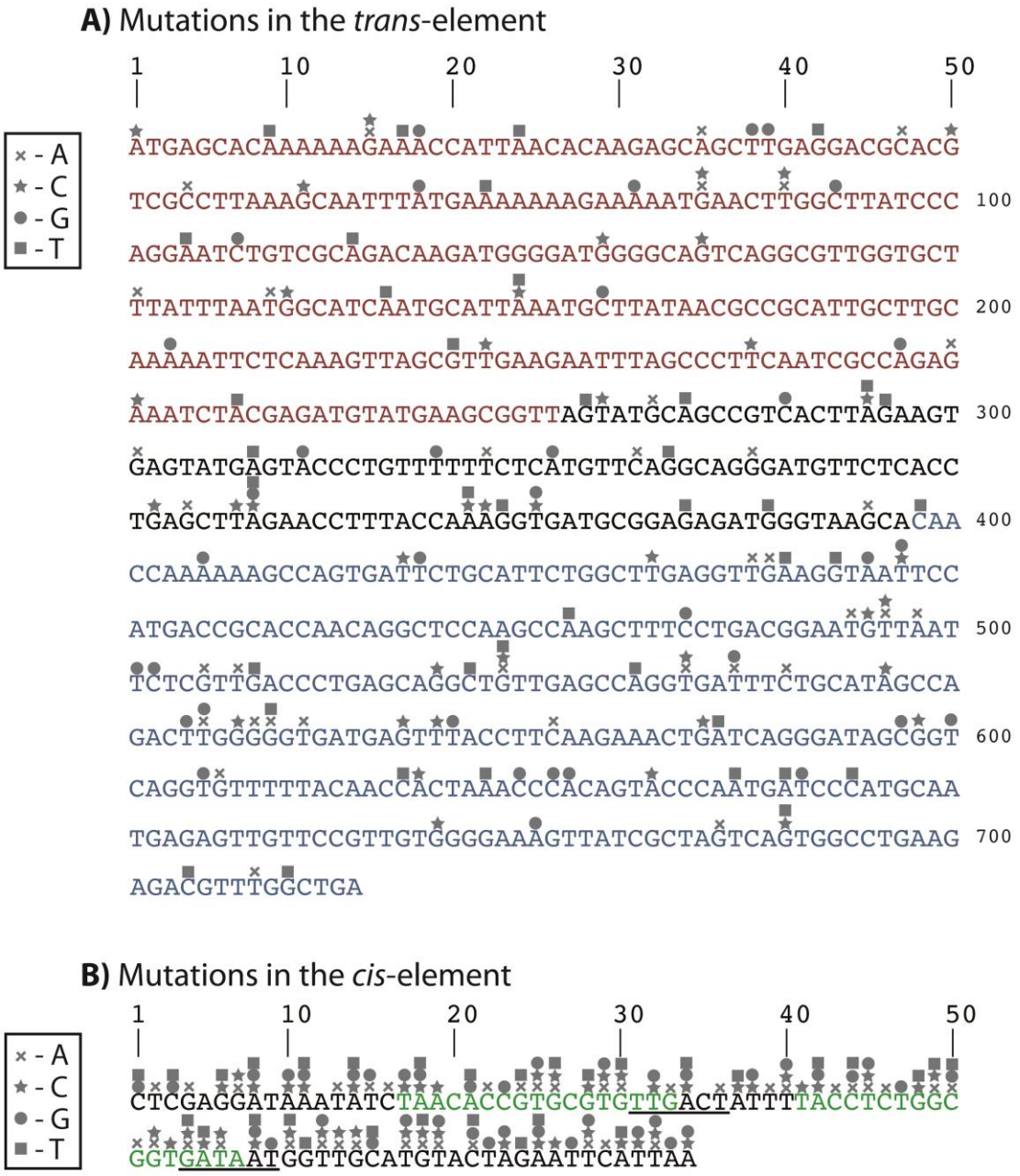

Figure 3 – Figure Supplement 2

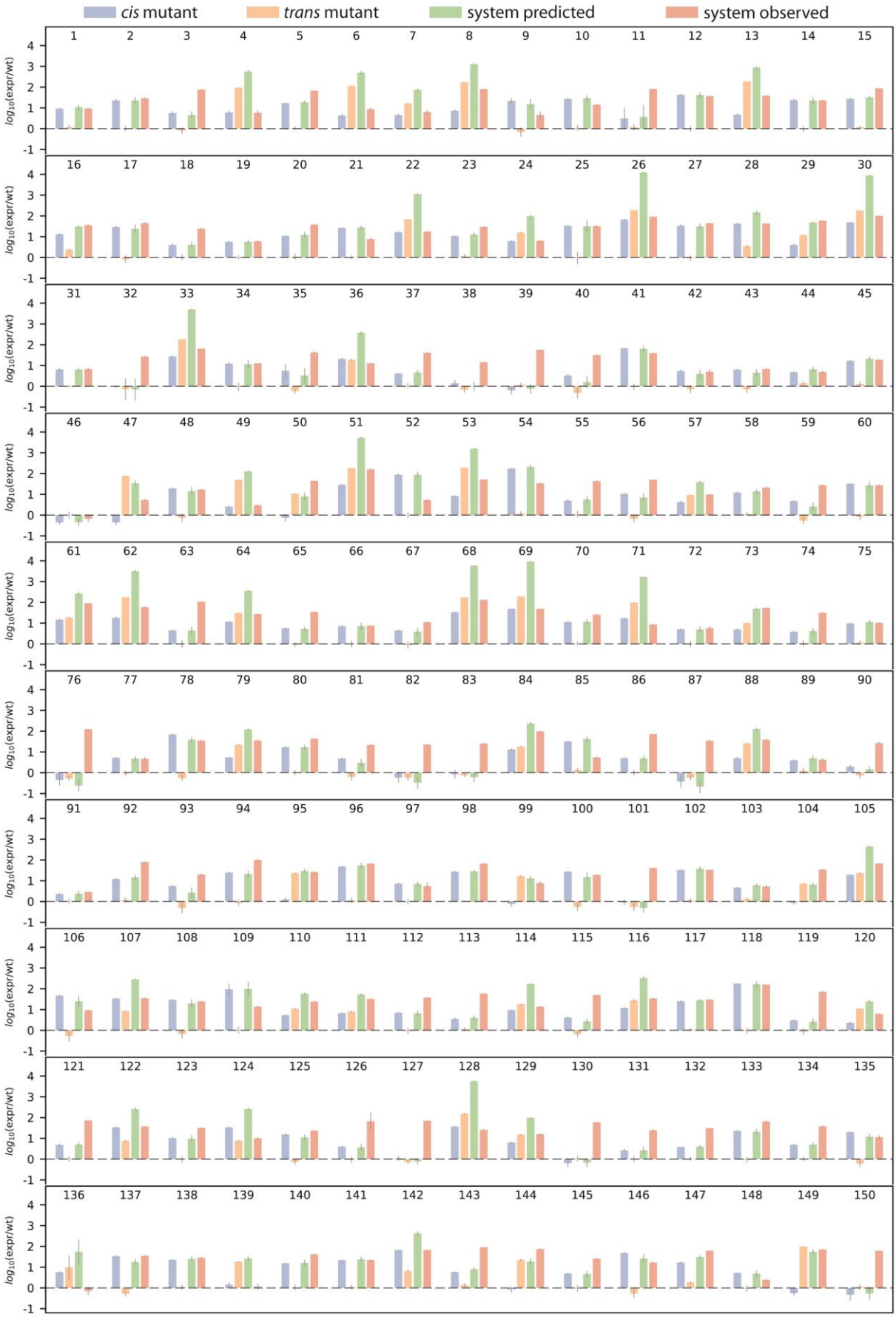

Figure 3 – Figure Supplement 3

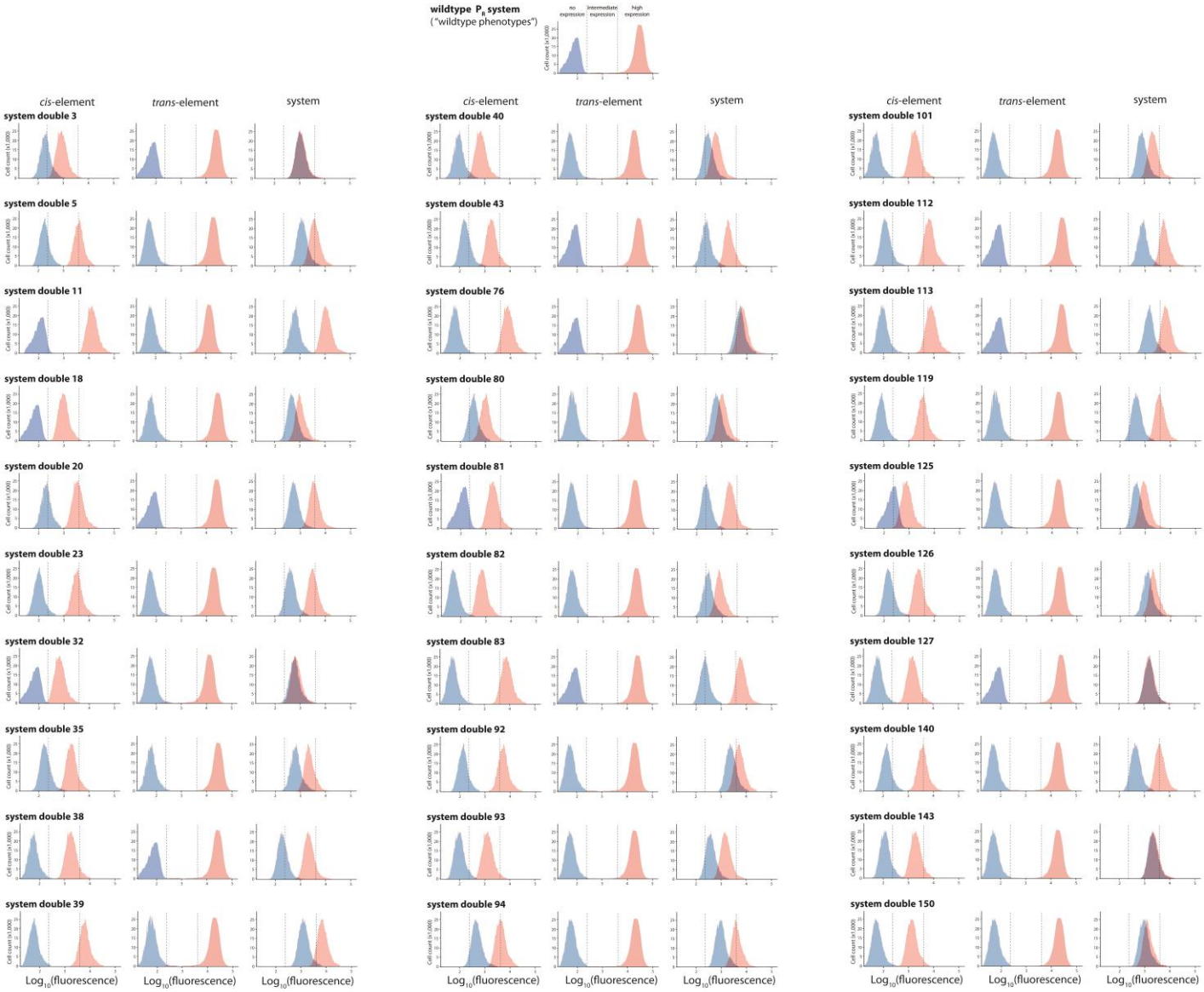

Figure 3 – Figure Supplement 4

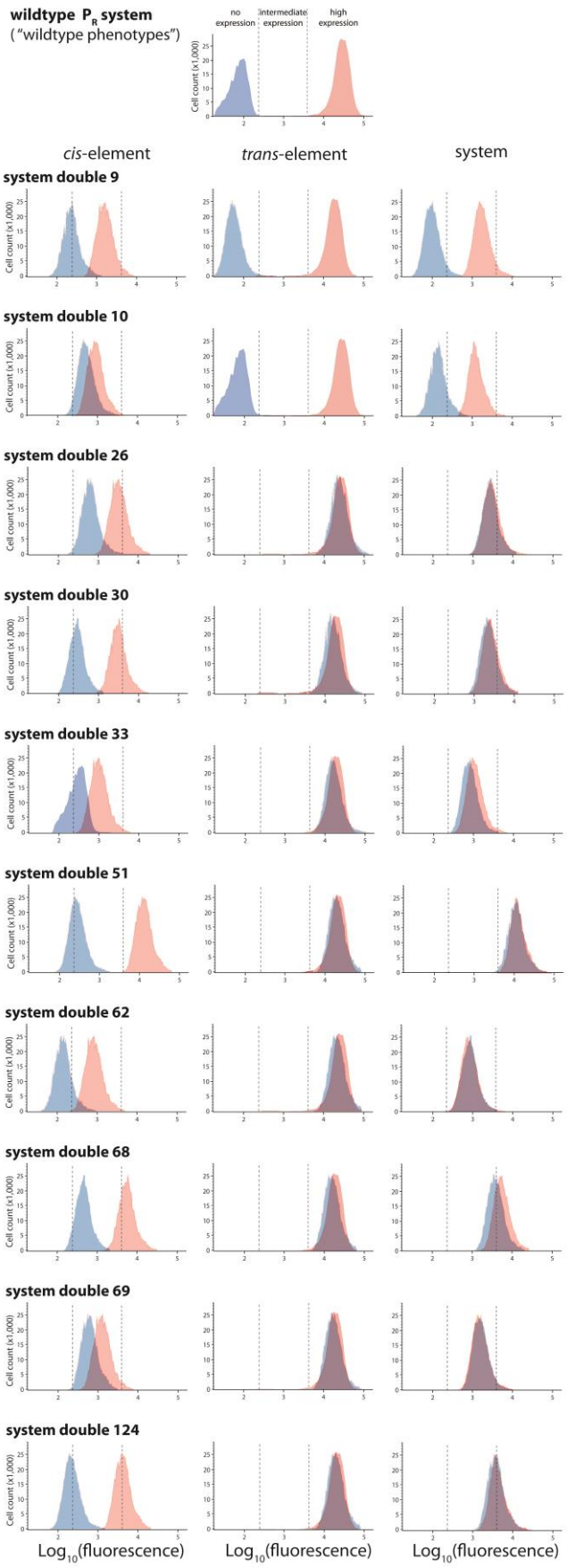

Figure 3 – Figure Supplement 5

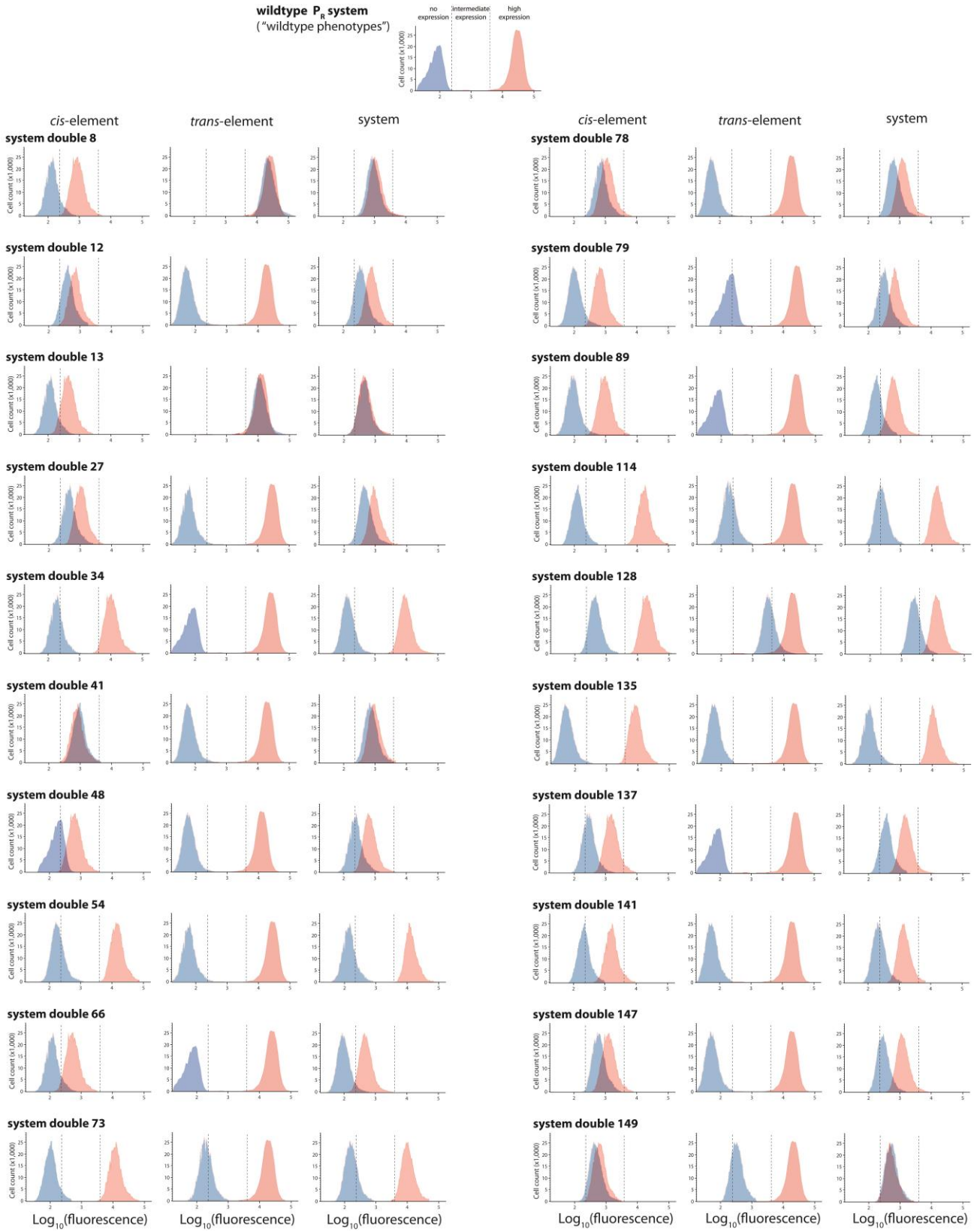

Figure 3 – Figure Supplement 6

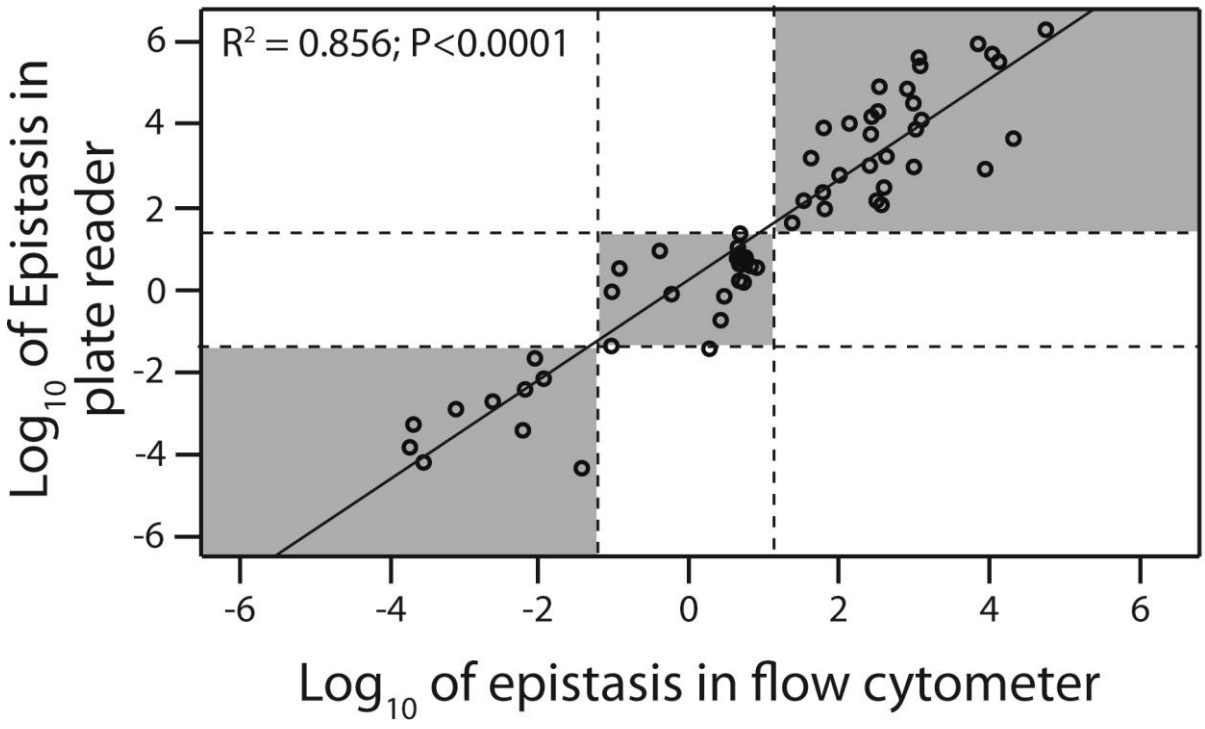

Figure 6 – Figure Supplement 1

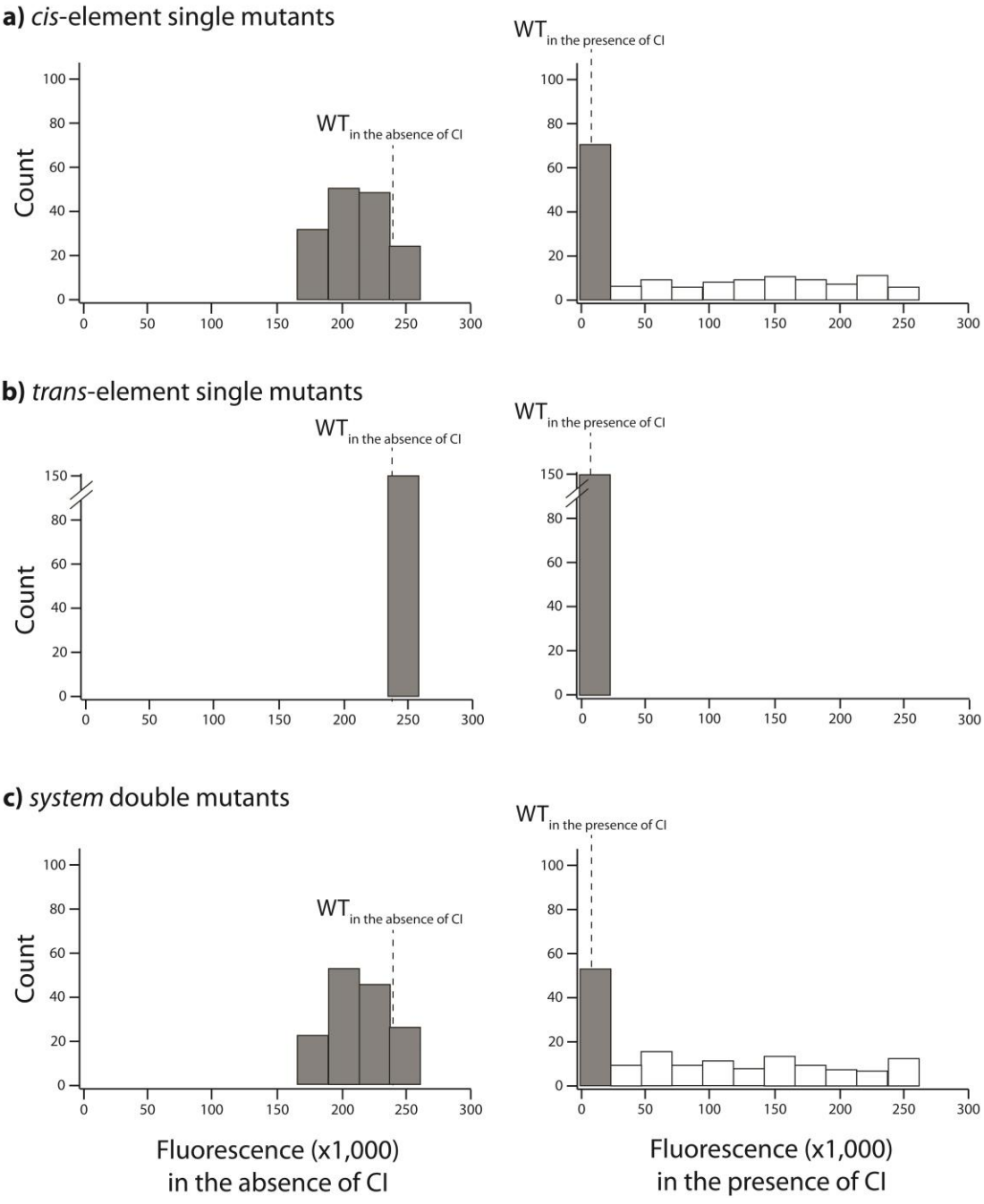

Figure 6 – Figure Supplement 2